Approximate Riemann Solvers, Godunov Schemes, and Contact Discontinuities

Burton Wendroff*
Retired Fellow and Associate, Los Alamos National Laboratory
Adjunct Professor, University of New Mexico

Abstract

This presentation divides logically into three parts. In Part I we briefly review the one-dimensional (1D) 3-state approximate Riemann solver (HLL) of [A. Harten, P. D. Lax and B. van Leer, *On upstream differencing and Godunov-type schemes for hyperbolic conservation laws*, SIAM Rev., 25 (1983), pp. 35-61], and its implementation (HLLE) of [B. Einfeldt, *On Godunov-type methods for gas dynamics*, SIAM J. Numer. Anal., 25 (1988), pp. 294-318]. We propose here a two-dimensional (2D) 9-state approximate Riemann solver and a corresponding 2D Godunov scheme. The result of applying this to some 2D shock interaction problems studied in [C. W. Schulz-Rinne, J. P. Collins, and H. M. Glaz, *Numerical solution of the Riemann problem for two-dimensional gas dynamics*, SIAM J. Sci. Comput., 14 (1993), pp. 1394–1414] are shown.

In Part II we return to one dimension and review the 4-state contact-corrected version HLLC developed by Toro and others [E. F. Toro, *Riemann Solvers and Numerical Methods for Fluid Dynamics*, Springer, 1997]. This version preserves a stationary contact discontinuity exactly. Since, as is well known, the Lax-Friedrichs (LF) scheme can be considered a special case of HLL, but involving a single constant state rather than three, a 2-state contact corrected version LFC that has the same property is easily formulated. This can also be used as the predictor in a two step Lax-Wendroff scheme, leading to LWC. We show how LFC, LWC, and their composition, [R. Liska and B. Wendroff, *Composite schemes for conservation laws*, SIAM J. Numer. Anal., 35 (1998), pp. 2250-2271], behave on some of the test problems in Toro's book.

In Part III we explore the possibility of extending the contact correction to two dimensions. The easiest way to do this is by dimensional splitting and the result of this is shown on a two dimensional shock contact interaction problem, also from the work of Schulze-Rinne et al. A truly two-dimensional 4-state extension of LFC is feasible and the result of this for the same interaction problem is shown. In principle HLLC could be formulated in two dimensions using the same construction as was used for HLLE, but this would involve 16 constant states and the associated Godunov scheme would likely be very inefficient.

1 Introduction

There are three parts to this work. Part I is concerned with approximate Riemann solvers and associated Godunov schemes in one and two dimensions. In section 2 we briefly review the one-dimensional (1D) 3-state approximate Riemann solver and associated Godunov scheme HLL of Harten, Lax, and van Leer [4] and its implementation HLLE of of Einfeldt [2]. In section 3 we show what a truly two-dimensional (2D) Godunov's method would be if one could solve 2D Riemann problems exactly. We then present several nine-state 2D versions of HLLE in section 3.1. We did this for the four-quadrant Riemann problem, but in principle this could be done for other configurations. The associated Godunov scheme is outlined, and then some computational details are described in section 3.2. In section 4 we present the result of two calculations, namely, cases 3 and 4 from [8]. These are four-shock configurations and were chosen simply to show that our 2D HLLE scheme is consistent with the solution of these problems obtained by more accurate means.

In Part II we return to 1D and consider the 4-state contact-corrected version HLLC developed by Toro and others [10] This version preserves a stationary contact discontinuity exactly. Since, as is well known, the Lax-Friedrichs (LF) scheme can be considered a special case of HLL, but involving a single constant state rather than three, a 2-state contact corrected version LFC that has the same property is easily formulated. This can also be used as the predictor in a two step Lax-Wendroff scheme, leading to LWC. We show how LFC, LWC, and their

*(bbw@lanl.gov, http://math.unm.edu/~bbw). This research is supported by the Department of Energy, under contract W-7405-ENG-36 and the CHAMMP Program.

composition behave on some of the test problems in Toro's book. However, we show by some examples that exact stationary contact preservation is not always a good thing.

In Part III we explore the possibility of extending the contact correction to two dimensions. The easiest way to do this is by dimensional splitting and we show the result of this on a two dimensional shock contact interaction problem, also from the work of Schulze-Rinne et al. A truly two-dimensional 4-state extension of LFC is feasible and the result of this for the same interaction problem is shown. Figure 19 shows that there are difficulties with this particular formulation. In principle HLLC could be formulated in two dimensions using the same construction as was used for HLLE, but this would involve 16 constant states and the associated Godunov scheme would likely be very inefficient.

2 Godunov's Method

We begin with a review of Godunov's original method, following [2]. Consider the system of conservation laws

$$v_t + f_x(v) = 0,$$

where

$$v = \begin{pmatrix} \rho \\ m \\ E \end{pmatrix}, \quad f(v) = \begin{pmatrix} m \\ \frac{m^2}{\rho} + p \\ \frac{m}{\rho}(E+p) \end{pmatrix}.$$

The gas dynamic state consists of the density ρ, the velocity q, and internal energy density e. Then $m = \rho q$, $E = \rho(e + \frac{1}{2}q^2)$, and the pressure p is given by an equation of state, $p = p(\rho, e)$. We restrict ourselves to the ideal gas equation of state, p$=(\gamma - 1)\rho e$.

The integral form of the conservation law is

$$\int_a^b v(x,t_1)\ dx = \int_a^b v(x,t_0)\ dx - \int_{t_0}^{t_1} f(v(b,s))\ ds + \int_{t_0}^{t_1} f(v(a,s))\ ds \tag{1}$$

for any $a < b$ and $0 \leq t_0 < t_1$.

The Riemann problem (centered at x_0, t_0) asks for the solution of (1) with initial data

$$v(x,t_0) = \begin{cases} u_0, & x < x_0 \\ u_1, & x > x_0 \end{cases}. \tag{2}$$

The solution is a function of $(x - x_0)/(t - t_0)$,

$$\omega((x - x_0)/(t - t_0)) \tag{3}$$

The structure of this solution is well-known. A description in terms of elementary waves (shock, contact or rarefaction), and an algorithm for solving the nonlinear equations defining the solution can be found in [10]. A rigorous mathematical treatment is in [9].

The Godunov scheme for general initial data is first to approximate the initial states by piecewise constant states, then use the solution of the local Riemann problems to construct new piecewise constant states by averaging. Thus, suppose we have a grid with cell centers $x_i = i\Delta x$, $i = 0, \pm 1, \pm 2, \cdots$, cell endpoints $x_{i+\frac{1}{2}} = (i + \frac{1}{2})\Delta x$ and discrete time steps $t^n = n\Delta t$. Then given

$$v_i^n = \frac{1}{\Delta x}\int_{x_{i-\frac{1}{2}}}^{x_{i+\frac{1}{2}}} v(x,t^n)\ dx$$

Godunov defines v_i^{n+1} by

$$v_i^{n+1} = \frac{1}{\Delta x}\int_0^{\frac{\Delta x}{2}} \omega_{i-\frac{1}{2}}^n(x/\Delta t)\ dx + \frac{1}{\Delta x}\int_{-\frac{\Delta x}{2}}^0 \omega_{i+\frac{1}{2}}^n(x/\Delta t)\ dx, \tag{4}$$

where $\omega_{i-\frac{1}{2}}^n((x - x_{i-\frac{1}{2}})/(t - t^n))$ is the solution of (1 and (2) centered at $(x_{i-\frac{1}{2}}, t^n)$ and with $u_0 = v_{i-1}^n,\ u_1 = v_i^n$. Since an exact Riemann solution is used, it follows from (1) that there is a numerical flux F such that

$$v_i^{n+1} = v_i^n - \lambda(F_{i+\frac{1}{2}}^n - F_{i-\frac{1}{2}}^n), \tag{5}$$

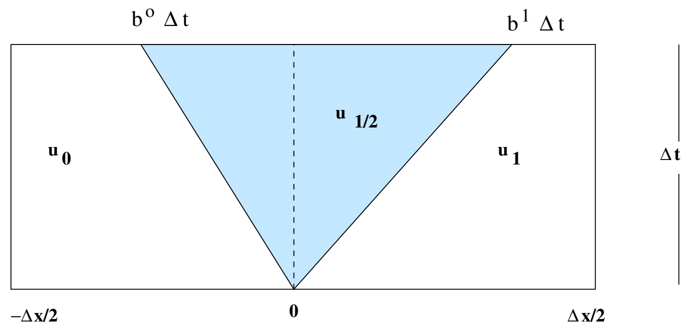

Figure 1: Structure of the HLLE solution

.

where

$$F^n_{i+\frac{1}{2}} = f(\omega^n_{i+\frac{1}{2}}(0)), \tag{6}$$

and

$$\lambda = \frac{\Delta t}{\Delta x},$$

and therefore the integrals in (4) do not have to be computed.

2.1 HLLE

The approximate solution of (2) proposed by Einfeldt [2], based on the HLL solver of Harten, Lax and van Leer [4], and now known as the HLLE solver consists of two speeds, $b^0 < b^1$, the two initial states u_0 and u_1, and a third intermediate state $u_{\frac{1}{2}}$. Then an approximate ω is (for $x_0 = 0$, $t_0 = 0$)

$$\omega(x/t) = \begin{cases} u_0, \ x < b^0 t \\ u_{\frac{1}{2}}, \ b^0 t < x < b^1 t \\ u_1, \ x > b^1 t \end{cases}, \tag{7}$$

where the left and right speeds $b^0 < b^1$ and the intermediate state $u_{\frac{1}{2}}$ are to be determined. The speeds are meant to be approximations to the smallest and largest signal velocities of the exact Riemann problem. Einfeldt assumes that

$$\Delta t \max(|b^0|, |b^1|) \leq \Delta x/2. \tag{8}$$

The intermediate state is defined to satisfy the integral conservation law in the interval $(-\Delta x/2, \Delta x/2)$, that is,

$$\int_{-\Delta x/2}^{\Delta x/2} \omega(x'/t)\ dx = \frac{\Delta x}{2}(u_0 + u_1) - \Delta t(f(u_1) - f(u_0)),$$

or

$$u_{\frac{1}{2}} = \frac{b^1 u_1 - b^0 u_0 + f(u_0) - f(u_1)}{b^1 - b^0}. \tag{9}$$

Figure 1 shows the space time structure of the approximate solution. For simplicity, the figure is drawn assuming that $b^0 \leq 0$ and $b^1 \geq 0$.

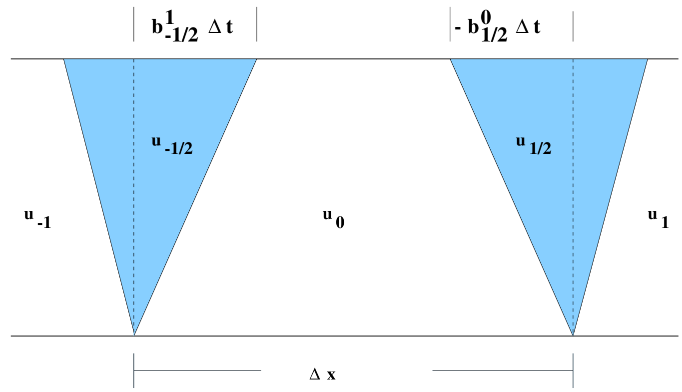

Figure 2: The HLLE-Godunov scheme

.

The Godunov scheme at a generic mesh cell ($i = 0$) advances the state u_0 to its new value u_0^1 according to

$$\Delta x u_0^1 = b^1_{-\frac{1}{2}} \Delta t u_{-\frac{1}{2}} - b^0_{\frac{1}{2}} \Delta t u_{\frac{1}{2}} + (\Delta x - (b^1_{-\frac{1}{2}} - b^0_{\frac{1}{2}})\Delta t) u_0$$

as in Figure 2.

However, just as in the exact case, there is a flux form. For the full set of difference equations we have (5) with

$$F_{i+\frac{1}{2}} = \frac{b^+_{i+\frac{1}{2}} f(v_i) - b^-_{i+\frac{1}{2}} f(v_{i+1})}{b^+_{i+\frac{1}{2}} - b^-_{i+\frac{1}{2}}} + \frac{b^+_{i+\frac{1}{2}} b^-_{i+\frac{1}{2}}}{b^+_{i+\frac{1}{2}} - b^-_{i+\frac{1}{2}}} (v_{i+1} - v_i), \tag{10}$$

where

$$b^+_{i+\frac{1}{2}} = \max(0, b^1_{i+\frac{1}{2}}), \qquad b^-_{i+\frac{1}{2}} = \min(0, b^0_{i+\frac{1}{2}}). \tag{11}$$

The speeds remain to be chosen. The speeds proposed in [2] are defined in Appendix A for the 2D gas dynamic equations in terms of Roe averages. For the 1D system here just suppress the second index, j, and set $q^x = q$, $q^y = 0$.

2.2 Stability, entropy, and positivity

The derivation of the exact and approximate Godunov schemes assumes that waves generated at the cell endpoints do not interact during one time step, that is, that (8) holds . In fact, as pointed out in [4], the exact Godunov scheme is valid as long as waves from one endpoint do not reach an adjacent endpoint in one time step. A similar situation holds for the HLLE scheme, in that there is a stability condition derived in [2] that is less restrictive than (8). To review this condition, suppose that f' is a constant matrix A, with eigenvalues $\beta_1 < \beta_2 < \beta_3$. Then

$$b^0 = b^0_{i+\frac{1}{2}} = \beta_1, \qquad b^1 = b^1_{i+\frac{1}{2}} = \beta_3,$$

and

$$v_i^{n+1} = (1 - \lambda\sigma) v_i^n + \frac{1}{2}\lambda(\sigma + A) v_{i-1}^n + \frac{1}{2}\lambda(\sigma - A) v_{i+1}^n,$$

where

$$\sigma = \frac{A(b^+ + b^-) - 2b^+ b^-}{b^+ - b^-}. \tag{12}$$

By construction, $\sigma \pm A \geq 0$, so all coefficients are positive if $\lambda\sigma \leq 1$, which is the case if

$$\max(b^+, -b^-)\lambda \leq 1. \tag{13}$$

It is shown in [3] that both the HLLE scheme with its stability condition and the exact Godunov scheme are positivity-conserving, that is, if the density and internal energy are initially positive then they are for all time. We refer the reader to [4] for a definition and discussion of entropy and the entropy inequality. It is shown there that exact Godunov satisfies the entropy inequality, and that a scheme like HLLE does also if the speeds b^0 and b^1 bound the exact wave speeds. According to [1] this is not always the case for the choice for the chosen speeds,thus, the behavior of entropy for HLLE is unknown.

3 Godunov and HLLE in Two Dimensions

The system of conservation laws is

$$v_t + f_x(v) + g_y(v) = 0,$$

where

$$v = \begin{pmatrix} \rho \\ m \\ n \\ E \end{pmatrix}, \quad f(v) = \begin{pmatrix} m \\ \frac{m^2}{\rho} + p \\ \frac{mn}{\rho} \\ \frac{m}{\rho}(E+p) \end{pmatrix}, \quad g(v) = \begin{pmatrix} n \\ \frac{mn}{\rho} \\ \frac{n^2}{\rho} + p \\ \frac{n}{\rho}(E+p) \end{pmatrix}, \tag{14}$$

where if q^x, q^y are respectively the x and y components of velocity then $m = \rho q^x$, $n = \rho q^y$, $E = \rho(e + \frac{1}{2}((q^x)^2 + (q^y)^2))$, and p and e are pressure and internal energy, as before.

The integral form of the conservation law, specifically for rectangles, is

$$\begin{aligned} &\int_a^b \int_c^d v(x,y,t_1) dxdy = \int_a^b \int_c^d v(x,y,t_0)\ dxdy \\ &- \int_{t_0}^{t_1} \int_c^d f(v(b,y,s))\ dyds + \int_{t_0}^{t_1} \int_c^d f(v(a,y,s))\ dyds \\ &- \int_{t_0}^{t_1} \int_a^b g(v(x,d,s))\ dxds + \int_{t_0}^{t_1} \int_a^b g(v(x,c,s))\ dxds \end{aligned} \tag{15}$$

for any $a < b$, $c < d$ and $0 \le t_0 < t_1$.

There is an infinite variety of two-dimensional Riemann problems, but only one type which is relevant for a rectangular grid, namely, the four quadrant problem (centered at x_0, y_0, t_0), that is, find $v(x,y,t)$ satisfying (15) with initial data

$$v(x,y,t_0) = \begin{cases} u_{00}, & x < x_0,\ y < y_0 \\ u_{01}, & x < x_0,\ y > y_0 \\ u_{11}, & x > x_0,\ y > y_0 \\ u_{10}, & x > x_0,\ y < y_0 \end{cases}. \tag{16}$$

Unlike the situation in one dimension, where everything is known about the Riemann problem, here almost nothing is known. The complexity of the solution can be seen from the numerical results of [8]. Nevertheless, we can proceed formally and suppose a solution which is a function of $((x-x_0)/(t-t_0), (y-y_0)/(t-t_0))$,

$$\omega((x-x_0)/(t-t_0), (y-y_0)/(t-t_0)). \tag{17}$$

A literal extension of Godunov's idea for general initial data in two dimensions is first to approximate the initial states by piecewise constant states, then use the solution of the two-dimensional local Riemann problems to construct new piecewise constant states by averaging. Thus, suppose we have a uniform rectangular grid with cell centers $x_i = i\Delta x$, $y_j = j\Delta y$, $i, j = 0, \pm 1, \pm 2, \cdots$, cell vertices $x_{i+\frac{1}{2}} = (i + \frac{1}{2})\Delta x$, $y_{j+\frac{1}{2}} = (j + \frac{1}{2})\Delta y$ and discrete time steps $t^n = n\Delta t$.

Call the $\Delta x \times \Delta y$ cells centered on the vertices the *dual* cells, and call the original cells the *primary cells.* The cell arrangement and the Riemann data are shown in Figure 3.

Then given piecewise-constant data in the primary cells, namely,

$$v_{i,j}^n = \frac{1}{\Delta x \Delta y} \int_{x_{i-\frac{1}{2}}}^{x_{i+\frac{1}{2}}} \int_{y_{j-\frac{1}{2}}}^{y_{j+\frac{1}{2}}} v(x,y,t^n)\ dydx$$

we could define $v_{i,j}^{n+1}$ by solving the 2D Riemann problem in each dual cell and projecting these solutions onto the primary cells, obtaining

$$v_{i,j}^{n+1} \quad = \quad \frac{1}{\Delta x \Delta y} \int_0^{\frac{\Delta x}{2}} \int_0^{\frac{\Delta y}{2}} \omega_{i-\frac{1}{2},j-\frac{1}{2}}^n (x/\Delta t, y/\Delta t)\ dydx$$

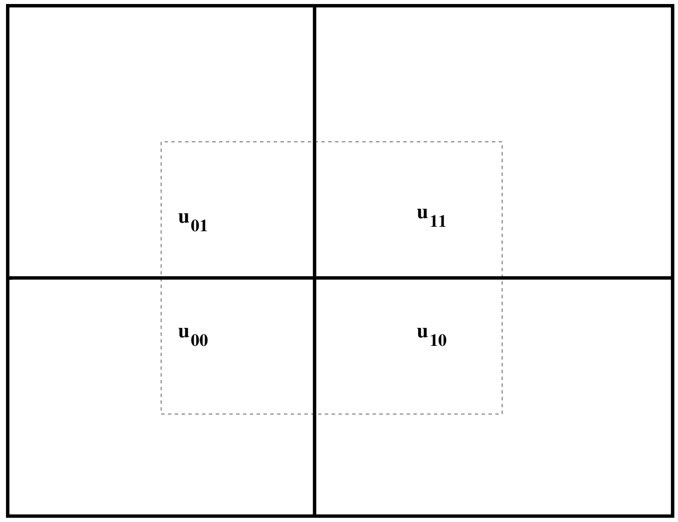

Figure 3: Primary (dark lines) and dual (dotted lines) cell arrangement with Riemann data

.

$$
\begin{aligned}
&+\frac{1}{\Delta x\Delta y}\int_{0}^{\frac{\Delta x}{2}}\int_{-\frac{\Delta y}{2}}^{0}\omega^n_{i-\frac{1}{2},j+\frac{1}{2}}(x/\Delta t, y/\Delta t)\ dydx\\
&+\frac{1}{\Delta x\Delta y}\int_{-\frac{\Delta x}{2}}^{0}\int_{-\frac{\Delta y}{2}}^{0}\omega^n_{i+\frac{1}{2},j+\frac{1}{2}}(x/\Delta t, y/\Delta t)\ dydx\\
&+\frac{1}{\Delta x\Delta y}\int_{-\frac{\Delta x}{2}}^{0}\int_{0}^{\frac{\Delta y}{2}}\omega^n_{i+\frac{1}{2},j-\frac{1}{2}}(x/\Delta t, y/\Delta t)\ dydx
\end{aligned}
\tag{18}
$$

where

$$
\omega^n_{i-\frac{1}{2},j-\frac{1}{2}}((x-x_{i-\frac{1}{2}})/(t-t^n),(y-y_{j-\frac{1}{2}})/(t-t^n))
$$

is the solution of (15) and (16) centered at $(x_{i-\frac{1}{2}}, y_{j-\frac{1}{2}}, t^n)$ and with $u_{00} = v^n_{i-1,j-1}$, $u_{01} = v^n_{i-1,j}$, $u_{11} = v^n_{i,j}$, $u_{10} = v^n_{i,j-1}$.

This construction only makes sense if waves generated by the 2D Riemann problems in any dual cells do not interact with the waves from its neighbors. So if σ is the maximum signal speed, maximized over all directions and all vertices, then we require $\sigma\Delta t < \min(\Delta x/2, \Delta y/2)$.

3.1 Some nine-state Riemann solvers

Unfortunately, the preceding section does not define a numerical method since there is no possibility of solving (16) exactly. This can be seen in [8], where it is shown that even the simplest nontrivial 2D Riemann problems have extremely complex solutions. So let us consider what an approximate solution might look like in Figure 4. This is a schematic of a dual cell after a small time interval of evolution of the 2D Riemann problem. Because signals propagate with finite speed, the cell can be divided into nine pieces of three different types, R_0, R_1, and R_2. In the corner R_0 regions the data are undisturbed from their initial states. In the edge R_1 regions the states are completely determined by the associated 1D Riemann problems. The central region R_2 contains the 2D interaction.

In analogy with the one-dimensional case, our two-dimensional HLLE solution will define nine specific regions in terms of speeds, and then assign a constant state to each of the nine regions. There are several ways to do this, but in each instance the four corner regions will have their initial values, in the edge strips the constant state will be the intermediate state obtained from a one-dimensional HLLE solver, and then the integral conservation law (15) will be used to define the central constant state.

Consider first Figure 5a. This shows a possible nine state configuration (Method 1) in which points on opposite edges of the cell have been joined by straight lines. The points on the edges will be defined by 1D HLLE speeds. This method is rather inefficient as it requires computation of intersections of lines and areas of quadrilaterals.

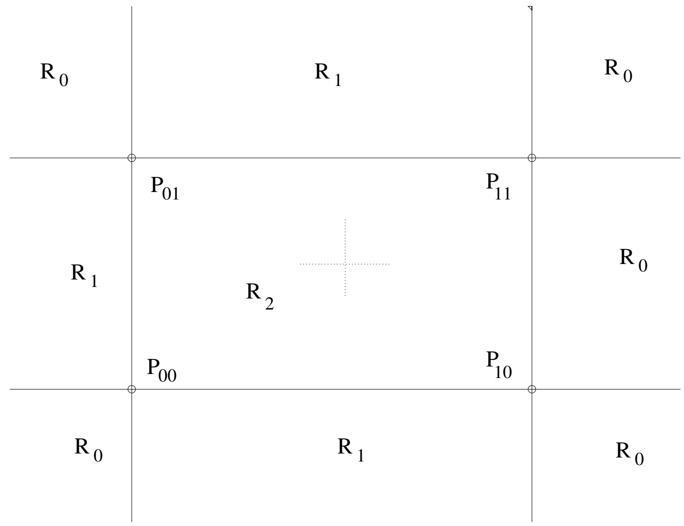

Figure 4: Structure of the 2D solution at later time. Dotted lines indicate initial center of the Riemann problem
.

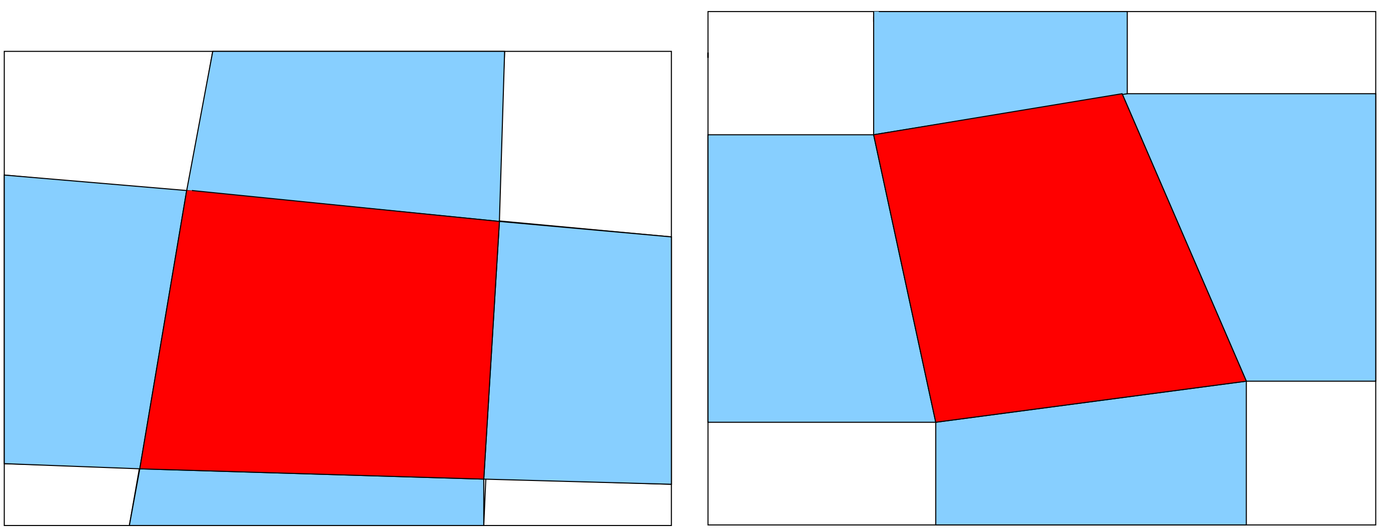

a) b)

Figure 5: a): Method 1, direct connection to edges. b) Method 2, trapezoidal edge sets, quadrilateral central set

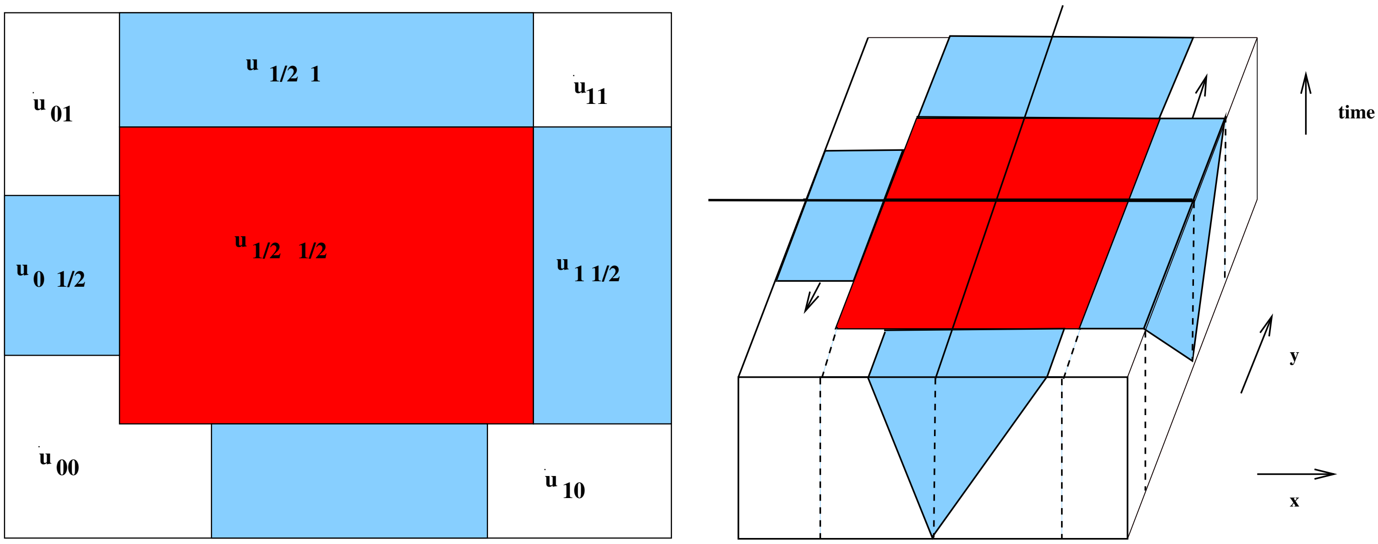

a) b)

Figure 6: a): Method 3, rectangular sets. b) Space-time structure for Method 3

.

A second possibility (Method 2) is shown in Figure 5b. Again, the points on the edges are defined by 1D HLLE speeds, but now the corner regions are rectangles and the edge strips are trapezoids. This is the construction used in [12].

A third arrangement (Method 3) is shown in Figure 6a. Here, the edge and central regions are rectangles. This is slightly less efficient than the second method above, but it has the advantage that there is a formula, (43), for the value of the central state that clearly is a generalization of (9). There also is a flux form, but it is very complicated and only of possible theoretical use. Figure 6b is a sketch of the time evolution of this approximate Riemann solver.

Consider only the latter two methods. The regions of constancy will depend on the 1D Einfeldt speeds.

Consider the cell vertex at $(x_{\frac{1}{2}}, y_{\frac{1}{2}})$. The four states interacting at this vertex are (suppressing the time index) $u_{00} = v_{0,0},\ u_{10} = v_{1,0},\ u_{11} = v_{1,1},\ u_{01} = v_{0,1}$. For Method 2 ideally we would like to use the following velocities to define the central region:

$$
\begin{aligned}
b^{01}_{\frac{1}{2},\frac{1}{2}} &= (b^{0}_{\frac{1}{2},1}, b^{1}_{0,\frac{1}{2}}),\\
b^{11}_{\frac{1}{2},\frac{1}{2}} &= (b^{1}_{\frac{1}{2},1}, b^{1}_{1,\frac{1}{2}}),\\
b^{10}_{\frac{1}{2},\frac{1}{2}} &= (b^{1}_{\frac{1}{2},0}, b^{0}_{1,\frac{1}{2}}),\\
b^{00}_{\frac{1}{2},\frac{1}{2}} &= (b^{0}_{\frac{1}{2},0}, b^{0}_{0,\frac{1}{2}}).
\end{aligned}
\tag{19}
$$

(See Appendix A for the detailed definition of these speeds). For example, $b^{0}_{\frac{1}{2},1}$ and $b^{1}_{\frac{1}{2},1}$ are the left and right HLLE speeds for the one-dimensional Riemann problem in the x-direction (with flux f) with $u_0 = v_{0,1}$ and $u_1 = v_{1,1}$, while $b^{0}_{0,\frac{1}{2}}$ and $b^{1}_{0,\frac{1}{2}}$ are the left and right HLLE speeds for the one-dimensional Riemann problem in the y-direction (with flux g) with $u_0 = v_{0,0}$ and $u_1 = v_{0,1}$.

However,since it is possible that $b^0 > 0$ or $b^1 < 0$, the corner rectangles might not be contained in their respective quadrants, as they are in Figure 4. If that happens the picture might in some cases not be as simple as shown and the computer code would have to be quite complicated in order to allow for this situation. Although it might be worth the extra work, in order to simply show the feasibility and consistency of the 2D HLLE scheme, we have chosen to avoid this difficulty at the cost of introducing somewhat more diffusion than is present in the 1D HLLE method. What is needed is to use (11) and replace (19) with

$$
b^{01}_{\frac{1}{2},\frac{1}{2}} = (b^{-}_{\frac{1}{2},1}, b^{+}_{0,\frac{1}{2}}),
$$

$$
\begin{aligned}
b^{11}_{\frac{1}{2},\frac{1}{2}} &= (b^{+}_{\frac{1}{2},1}, b^{+}_{1,\frac{1}{2}}),\\
b^{10}_{\frac{1}{2},\frac{1}{2}} &= (b^{+}_{\frac{1}{2},0}, b^{-}_{1,\frac{1}{2}}),\\
b^{00}_{\frac{1}{2},\frac{1}{2}} &= (b^{-}_{\frac{1}{2},0}, b^{-}_{0,\frac{1}{2}}).
\end{aligned}
\tag{20}
$$

The vertices of the interior quadrilateral (refer to Figure 4) are

$$
\begin{aligned}
P^{00}(t) &= (x_{\frac{1}{2}}, y_{\frac{1}{2}}) + b^{00}_{\frac{1}{2},\frac{1}{2}}(t - t^n),\\
P^{01}(t) &= (x_{\frac{1}{2}}, y_{\frac{1}{2}}) + b^{01}_{\frac{1}{2},\frac{1}{2}}(t - t^n),\\
P^{11}(t) &= (x_{\frac{1}{2}}, y_{\frac{1}{2}}) + b^{11}_{\frac{1}{2},\frac{1}{2}}(t - t^n),\\
P^{10}(t) &= (x_{\frac{1}{2}}, y_{\frac{1}{2}}) + b^{10}_{\frac{1}{2},\frac{1}{2}}(t - t^n).
\end{aligned}
$$

For method 3, define new velocities associated with $(x_{\frac{1}{2}}, y_{\frac{1}{2}})$

$$
\begin{aligned}
d^{x-} = d^{x-}_{\frac{1}{2},\frac{1}{2}} &= \min(b^{-}_{\frac{1}{2},1}, b^{-}_{\frac{1}{2},0}),\\
d^{x+} = d^{x+}_{\frac{1}{2},\frac{1}{2}} &= \max(b^{+}_{\frac{1}{2},1}, b^{+}_{\frac{1}{2},0}),\\
d^{y-} = d^{y-}_{\frac{1}{2},\frac{1}{2}} &= \min(b^{-}_{1,\frac{1}{2}}, b^{-}_{0,\frac{1}{2}}),\\
d^{y+} = d^{y+}_{\frac{1}{2},\frac{1}{2}} &= \max(b^{+}_{1,\frac{1}{2}}, b^{+}_{0,\frac{1}{2}})
\end{aligned}
$$

and then the four corners of the interior rectangle are

$$
\begin{aligned}
P^{00}(t) &= (x_{\frac{1}{2}}, y_{\frac{1}{2}}) + (d^{x-}, d^{y-})(t - t^n),\\
P^{01}(t) &= (x_{\frac{1}{2}}, y_{\frac{1}{2}}) + (d^{x-}, d^{y+})(t - t^n),\\
P^{11}(t) &= (x_{\frac{1}{2}}, y_{\frac{1}{2}}) + (d^{x+}, d^{y+})(t - t^n),\\
P^{10}(t) &= (x_{\frac{1}{2}}, y_{\frac{1}{2}}) + (d^{x+}, d^{y-})(t - t^n).
\end{aligned}
$$

We can now define the edge states (in the light shaded regions of Figs. 5a,b and 6a); namely $u_{0,\frac{1}{2}}$, $u_{\frac{1}{2},0}$, $u_{1,\frac{1}{2}}$, and $u_{\frac{1}{2},1}$. For example, $u_{0,\frac{1}{2}}$ is the HLLE intermediate state for the Riemann problem in the y-direction with $u_0 = u_{00}$ and $u_1 = u_{01}$ and with left speed $b^{-}_{0,\frac{1}{2}}$ and right speed $b^{+}_{0,\frac{1}{2}}$, and the others are defined similarly.

We can state the complete solution. Let $S_{\alpha,\beta}$ for $\alpha = 0, \frac{1}{2}, 1$, $\beta = 0, \frac{1}{2}, 1$ be the nine regions. Then

$$
\omega_{\frac{1}{2},\frac{1}{2}}(x,y) = u_{\alpha,\beta} \text{ for } (\mathrm{x}, \mathrm{y}) \in \mathrm{S}_{\alpha,\beta}.
\tag{21}
$$

The ninth state $u_{\frac{1}{2},\frac{1}{2}}$ is yet to be defined. Let $|S|_{\alpha,\beta}$ be the area of $S_{\alpha,\beta}$ at time $t = t^{n+1}$. Then based on (15) we can write the following approximate integral conservation form:

$$
\begin{aligned}
\sum_{\substack{\alpha = 0, \frac{1}{2}, 1\\ \beta = 0, \frac{1}{2}, 1}} |S|_{\alpha,\beta} u_{\alpha,\beta} &= \frac{\Delta x \Delta y}{4} \sum_{\substack{\alpha = 0, 1\\ \beta = 0, 1}} u_{\alpha,\beta}\\
&- \Delta y \Delta t (F_{1,\frac{1}{2}} - F_{0,\frac{1}{2}})\\
&- \Delta x \Delta t (G_{\frac{1}{2},1} - G_{\frac{1}{2},0}),
\end{aligned}
\tag{22}
$$

from which $u_{\frac{1}{2},\frac{1}{2}}$ can be obtained if $|S|_{\frac{1}{2},\frac{1}{2}} \neq 0$. The flux integrals will also be approximated using the 1D HLLE solutions. Note that (15) is being formulated over the space-time cell $C = \{x, y, t;\ x_0 \leq x \leq x_1,\ y_0 \leq y \leq y_1,\ t^n \leq t \leq t^{n+1}\}$. The flux integrals are integrals over the time-like faces of this cell. The structure of such a face is just as in Figure 1. Thus,

$$
\begin{aligned}
F_{0,\frac{1}{2}} &= \frac{1}{\Delta t \Delta y}[\frac{1}{2}(\Delta y - b^{+}_{0,\frac{1}{2}}\Delta t)\Delta t f(u_{01})\\
&+ \frac{1}{2}(\Delta y + b^{-}_{0,\frac{1}{2}}\Delta t)\Delta t f(u_{00})\\
&+ \frac{1}{2}(b^{+}_{0,\frac{1}{2}} - b^{-}_{0,\frac{1}{2}})(\Delta t)^2 f(u_{0,\frac{1}{2}})],
\end{aligned}
\tag{23}
$$

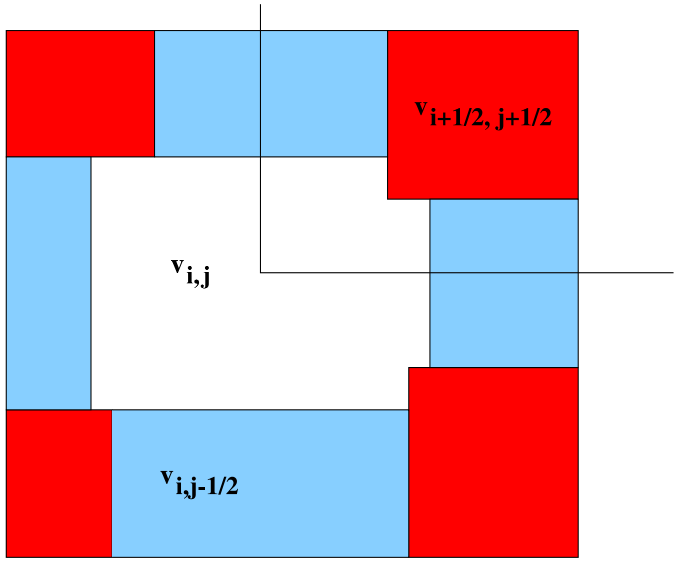

Figure 7: Primary cell

.

and

$$
\begin{aligned}
G_{\frac{1}{2},0} &= \frac{1}{\Delta t \Delta x}[\frac{1}{2}(\Delta x - b^{+}_{\frac{1}{2},0}\Delta t)\Delta t g(u_{10}) \\
&+ \frac{1}{2}(\Delta x + b^{-}_{\frac{1}{2},0}\Delta t)\Delta t g(u_{00}) \\
&+ \frac{1}{2}(b^{+}_{\frac{1}{2},j} - b^{-}_{\frac{1}{2},0})(\Delta t)^2 g(u_{\frac{1}{2},0})]. \qquad (24)
\end{aligned}
$$

3.2 The 2D HLLE-Godunov scheme

Just as with 1D in section 2.1, we use the approximate Riemann solution in place of the exact one in (18).

The computation can be organized into two phases

PHASE 1.

For each dual cell edge store the pair of speeds, the 1D intermediate state, and the fluxes F and G.

PHASE 2.

For each dual cell define the nine pieces, compute their areas, and then find the central intermediate state. Substitute the approximation given by (21) into (18) to obtain new constant states in the primary cells. This is quite easy since with (20) the corner sets Q_i in Fig. 4 lie entirely in their respective quadrants. For method 2 each edge set is a trapezoid which now splits into two trapezoids, each lying entirely in a quadrant. The area of the intersection of the dual cell central region with a quadrant (that is, with a neighboring primary cell) is simply what is left over from the other three pieces. Referring to the primary cell sketch in Figure 7, for method 3 the edge sets are rectangles which also split the same way, the corners of the primary cells are now simple rectangles (dark-shaded), and the undisturbed region of the primary cell is now just the complement of the union of the others. So the mapping onto the primary cells can be accomplished without a separate pass over the primary cells, by accumulating the contribution of each dual cell to its neighboring primary cells. In Figure 7, the states in the light-shaded regions are the 1D HLLE intermediate states determined by the adjacent cells, while the corner dark-shaded states come from the 2D interactions in the dual cells.

3.3 Stability

In Appendix B we present a flux form for method 3, that is, we show that

$$
v^{n+1}_{i,j} = v^{n}_{i,j} - \frac{\Delta t}{\Delta x}(\mathcal{F}_{i+\frac{1}{2},j} - \mathcal{F}_{i-\frac{1}{2},j}) - \frac{\Delta t}{\Delta y}(\mathcal{G}_{i,j+\frac{1}{2}} - \mathcal{G}_{i,j-\frac{1}{2}}). \qquad (25)
$$

These fluxes are complicated and we do not see a way to perform the kind of stability analysis done in 1D in [2]. However, we can look at the linear case in which f and g have constant gradient, matrices, $f' = A,\ g' = B$. Even this is difficult if these matrices don't commute. If we *assume* that $AB = BA$, with common eigenvalues $\beta_1 < \beta_2 = \beta_3 < \beta_4$, then all the left speeds are the same, and all the right speeds are the same, that is we can set

$$d^- = d^{x-}_{i+\frac{1}{2},j+\frac{1}{2}} = d^{y-}_{i+\frac{1}{2},j+\frac{1}{2}} = \min(\beta_1, 0),$$
$$d^+ = d^{x+}_{i+\frac{1}{2},j+\frac{1}{2}} = d^{y+}_{i+\frac{1}{2},j+\frac{1}{2}} = \max(\beta_4, 0).$$

In this case the three 2D HLLE schemes form the same nine-point scheme that is, in fact, the product of the 1D schemes. Let

$$(\mathrm{T_x v})_{\mathrm{i,j}} = \mathrm{v_{i+1,j}}, \quad (\mathrm{T_y v})_{\mathrm{i,j}} = \mathrm{v_{i,j+1}},$$

and

$$H_y = (\frac{1}{2}\lambda_y(\sigma_y - B)\mathrm{T_y} + (1-\sigma_\mathrm{y})\mathrm{I} + \frac{1}{2}\lambda_\mathrm{y}(\mathrm{B} - \sigma_\mathrm{y})\mathrm{T_y^{-1}}),$$
$$H_x = (\frac{1}{2}\lambda_x(\sigma_x - A)\mathrm{T_x} + (1-\sigma_\mathrm{x})\mathrm{I} + \frac{1}{2}\lambda_\mathrm{x}(\mathrm{A} - \sigma_\mathrm{x})\mathrm{T_x^{-1}}),$$

where $\lambda_x = \Delta t/\Delta x$, $\lambda_y = \Delta t/\Delta y$, and σ_x and σ_y are defined by (12) with the appropriate substitutions. Then

$$v^{n+1}_{i,j} = (H_x H_y v^n)_{i,j}$$

and in this very special case the 2D HLLE scheme is positive if (13) is satisfied.

For the numerical examples we used an adaptive time step determined by

$$\max(\lambda_x\kappa_x, \lambda_y\kappa_y) \le \mathrm{CFL} \le 1,$$

where κ_x, κ_y are the wave speeds in each direction. The maximum is taken over the grid as well as over the pair.

3.4 Entropy and positivity

There is little that can be said at this time about these difficult issues for the 2D HLLE scheme for gas dynamics, for several reasons. The computer program performing the operations described in section 3.2 is fairly simple, but the flux form of the finite difference scheme in terms of the speeds and the hydrodynamic states is very complicated, making an analysis of positivity extremely difficult. Concerning entropy, if we were using exact Riemann solvers for the 1D problems, exact integrals for the face fluxes and average intermediate states, and if the central region were guaranteed to contain all the 2D interactions, the convexity argument of [4] could presumably be used to establish an entropy inequality. Since none of these is the case, we are much worse off here concerning entropy than in 1D.

4 Numerical Examples

We have computed several of the 2D Riemann problems that were done in [8]. This set of problems was arranged so that the 1D interactions in each of them produce just one wave. We have chosen configurations 4 and 3 which are each four-shock interaction problems. The data are, using the indexing of (16), for configuration 4, γ=1.4, and

$$\begin{array}{lllll}
p_{00} & = & 1.1 & \rho_{00} = 1.1 & q^x_{00} = .8939 \quad q^y_{00} = .8939 \\
p_{01} & = & .35 & \rho_{01} = .5065 & q^x_{01} = .8939 \quad q^y_{01} = 0. \\
p_{11} & = & 1.1 & \rho_{11} = 1.1 & q^x_{11} = 0. \quad q^y_{11} = 0. \\
p_{10} & = & .35 & \rho_{10} = .5065 & q^x_{10} = 0. \quad q^y_{10} = .8939.
\end{array}$$

For configuration 3 the data are

$$\begin{array}{lllll}
p_{00} & = & .029 & \rho_{00} = .138 & q^x_{00} = 1.206 \quad q^y_{00} = 1.206 \\
p_{01} & = & .3 & \rho_{01} = .5323 & q^x_{01} = 1.206 \quad q^y_{01} = 0. \\
p_{11} & = & 1.5 & \rho_{11} = 1.5 & q^x_{11} = 0. \quad q^y_{11} = 0. \\
p_{10} & = & .3 & \rho_{10} = .5323 & q^x_{10} = 0. \quad q^y_{10} = 1.206.
\end{array}$$

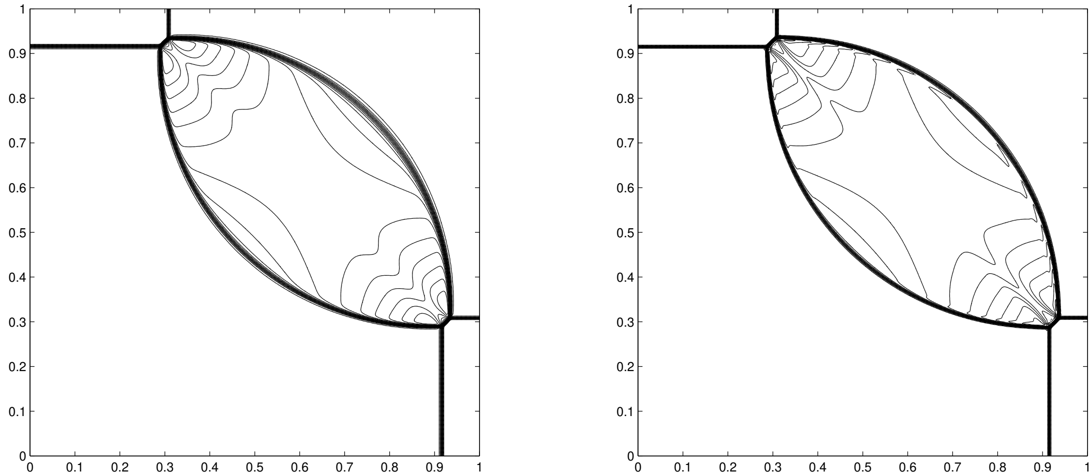

a) b)

Figure 8: Configuration 4. 400×400 grid, time=.25, cfl=.9, 30 density contours: a) 2D HLLE. b) CFLF4
.

All versions of 2D HLLE gave the same result. Density contours for configuration 4, using a grid 400×400, are shown in Figure 8. For comparison we show the same result for the composite scheme CFLF4, developed in [5]. We also show the density surface in Figure 9 for configuration 4 for the 2D HLLE scheme. This configuration probably has the least complicated 2D structure of them all, and 2D HLLE does very well on it.

Configuration 3 with the same grid is shown in Figure 10, along with the result of the composite CFLF4. This case has a more complex interaction, and some resolution is lost by the HLLE scheme. All computations were done with CFL=.9.

For case 4 all the left speeds b^0 were negative and all the right speeds b^1 were positive, but for case 3 some left speeds were positive (this is true for the initial data).

5 Contact Correction in 1D

We now take up Part II of this paper, which, as indicated in the introduction, is a return to problems with 1D symmetry. However, since this will also be used in a 2D splitting scheme, we will use the 2D flux f from (14). We are going to present 1D versions of the Lax-Friedrichs (LF)and Lax-Wendroff (LW) difference schemes for the gas dynamic equations that have an upwind feature, in the sense that at each grid point the flow direction is used to modify the difference equations. The idea is based on the approximate Riemann solver HLLC described in [10], Ch. 10, and we call these schemes LFC and LWC, respectively.

With the notation as in section 2, the two step LF scheme obtains the mean values v_i^{n+1} from the v_i^n according to the equations

$$v_{i+\frac{1}{2}}^{n+\frac{1}{2}} = .5(v_i^n + v_{i+1}^n) - .5\lambda(f(v_{i+1}^n) - f(v_i^n)) \tag{26}$$

and

$$v_i^{n+1} = .5(v_{i+\frac{1}{2}}^{n+\frac{1}{2}} + v_{i-\frac{1}{2}}^{n+\frac{1}{2}}) - .5\lambda(f(v_{i+\frac{1}{2}}^{n+\frac{1}{2}}) - f(v_{i-\frac{1}{2}}^{n+\frac{1}{2}})). \tag{27}$$

Note that this is just HLLE using maximal speeds and two half steps.

Let q^{x*} be the x-component of velocity extracted from $v_{i+\frac{1}{2}}^{n+\frac{1}{2}}$. That is

$$q^{x*} = m_{i+\frac{1}{2}}^{n+\frac{1}{2}} / \rho_{i+\frac{1}{2}}^{n+\frac{1}{2}}. \tag{28}$$

Define left and right densities ρ_l and ρ_r according to

$$\begin{aligned} \rho_l(\Delta x + q^{x*}\Delta t) &= \rho_i^n(\Delta x + (q^x)_i^n \Delta t), & (29)\\ \rho_r(\Delta x - q^{x*}\Delta t) &= \rho_{i+1}^n(\Delta x - (q^x)_{i+1}^n \Delta t). & (30) \end{aligned}$$

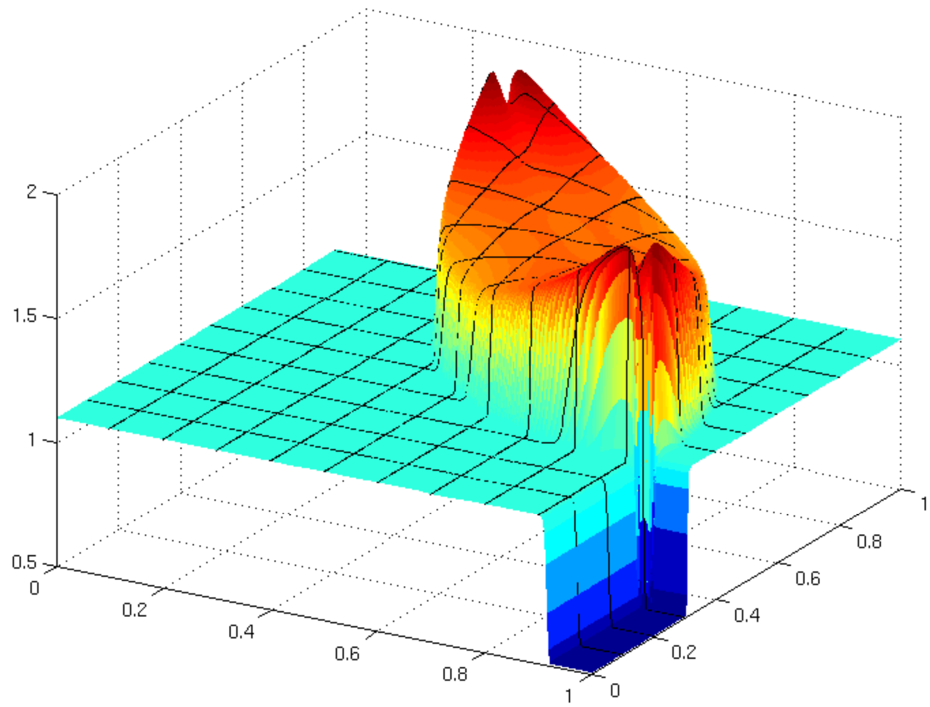

Figure 9: Density surface plot for configuration 4, 2DHLLE

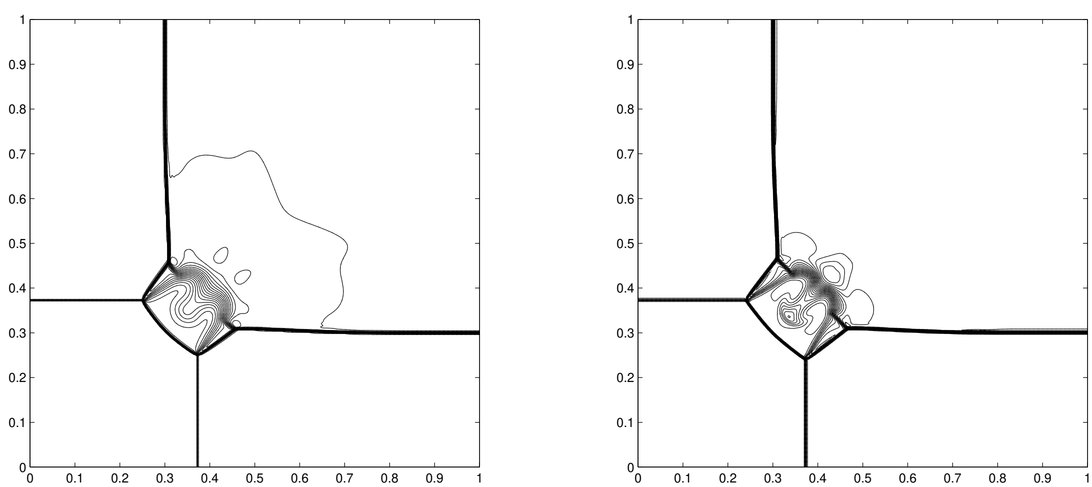

a) b)

Figure 10: Configuration 3. 400 $\times$ 400 grid, time=.3, cfl=.9, 30 contours: a) 2D HLLE. b) CFLF4

.

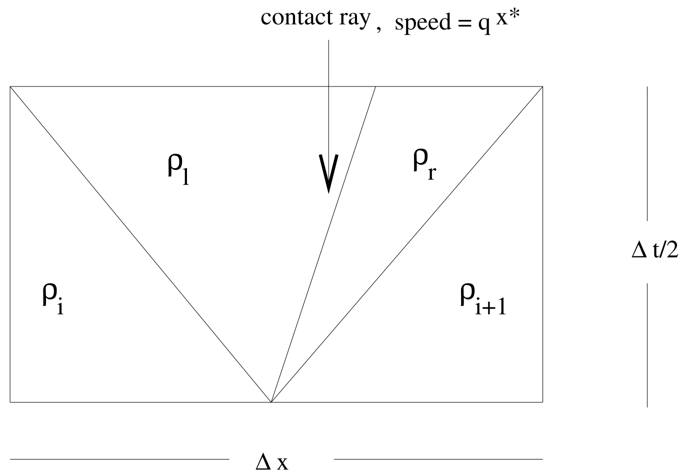

Figure 11: Contact ray and density distribution for LFC

.

This just amounts to assuming a contact discontinuity moving with speed q^{x*} as in Figure 11 and then splitting the mass flux into a left and right part. In the same way, the simply advected y-component of velocity splits according to

$$\begin{aligned}\rho_l q_l^y q^{x*}\Delta t + \Delta x) &= \rho_i^n (q^y)_i^n (\Delta x + (q^x)_i^n \Delta t),\\ \rho_r q_r^y (\Delta x - q^{x*}\Delta t) &= \rho_{i+1}^n (q^y)_{i+1}^n (\Delta x - (q^x)_{i+1}^n \Delta t).\end{aligned}$$

But then it follows from (30) that

$$q_l^y = (q^y)_i^n \quad \text{and} \quad \mathrm{q_r^y = (q^y)_{i+1}^n}.$$

The pressure $p*$ will also be extracted from $v_{i+\frac{1}{2}}^{n+\frac{1}{2}}$. However, special care has to be taken with the dependence of energy and pressure on the velocity component orthogonal to the direction of integration. This velocity is just advected in that direction with the fluid, but if the kinetic energy is computed using the average slip velocity then the pressure will be incorrect. This means we can't extract the pressure from the average energy using the kinetic energy of the average velocity field. Instead, we propose

$$p^* = (\gamma-1)(E_{i+\frac{1}{2}}^{n+\frac{1}{2}} - .5\rho_{i+\frac{1}{2}}^{n+\frac{1}{2}}(q^{x*})^2 - .25((1. + q^{x*}\lambda)\rho_l(q_l^y)^2 + (1. - q^{x*}\lambda)\rho_r(q_r^y)^2)). \tag{31}$$

Now replace (26) by

$$v_{i+\frac{1}{2}}^{n+\frac{1}{2}}(x) = \left\{ \begin{array}{ll} v_l, & x_i \le x \le x_{i+\frac{1}{2}} + q^{x*}\Delta t/2 \\ v_r, & x_{i+\frac{1}{2}} + q^{x*}\Delta t/2 \le x \le x_{i+1} \end{array} \right., \tag{32}$$

where

$$v_l = \begin{pmatrix} \rho_l \\ \rho_l q^{x*} \\ \rho_l q_l^y \\ \frac{p^*}{(\gamma-1)} + .5\rho_l[(q^{x*})^2 + (q_l^y)^2] \end{pmatrix}, \quad v_r = \begin{pmatrix} \rho_r \\ \rho_r q^{x*} \\ \rho_r q_r^y \\ \frac{p^*}{(\gamma-1)} + .5\rho_r[(q^{x*})^2 + (q_r^y)^2] \end{pmatrix}. \tag{33}$$

Then replace (27) by

$$v_i^{n+1} = \frac{1}{\Delta x}\int_{x_{i-\frac{1}{2}}}^{x_i} v_{i-\frac{1}{2}}^{n+\frac{1}{2}}(x)\ dx + \frac{1}{\Delta x}\int_{x_i}^{x_{i+\frac{1}{2}}} v_{i+\frac{1}{2}}^{n+\frac{1}{2}}(x)\ dx - \frac{1}{2}\lambda(f(v_{i+\frac{1}{2}}^{n+\frac{1}{2}}(x_{i+\frac{1}{2}})) - f(v_{i-\frac{1}{2}}^{n+\frac{1}{2}}(x_{i-\frac{1}{2}}))). \tag{34}$$

Then (32) and (34) define the scheme LFC. For LWC we simply set

$$v_i^{n+1} = v_i^n - \lambda(f(v_{i+\frac{1}{2}}^{n+\frac{1}{2}}(x_{i+\frac{1}{2}})) - f(v_{i-\frac{1}{2}}^{n+\frac{1}{2}}(x_{i-\frac{1}{2}}))). \tag{35}$$

5.1 1D numerical results

We have computed Toro's six test problems from Chapter 10 of [10] in Figures 12-14. The data are given below in the notation of (2). Recall that $q \equiv q^x$ is velocity, and here $q^y = 0$. For all problems, $\gamma = 1.4$.

Test 1:

$$\begin{aligned} p_0 &= 1. \quad \rho_0 = 1. \quad q_0 = .75 \\ p_1 &= .1 \quad \rho_1 = .125 \quad q_1 = 0. \end{aligned}$$

Test 2:

$$\begin{aligned} p_0 &= .4 \quad \rho_0 = 1. \quad q_0 = -2. \\ p_1 &= .4 \quad \rho_1 = 1. \quad q_1 = 2. \end{aligned}$$

Test 3:

$$\begin{aligned} p_0 &= 1000. \quad \rho_0 = 1. \quad q_0 = 0. \\ p_1 &= .01 \quad \rho_1 = 1. \quad q_1 = 0. \end{aligned}$$

Test 4:

$$\begin{aligned} p_0 &= 460.894 \quad \rho_0 = 5.99924 \quad q_0 = 460.894 \\ p_1 &= 46.095 \quad \rho_1 = 5.99242 \quad q_1 = 46.095 \end{aligned}$$

Test 5:

$$\begin{aligned} p_0 &= 1. \quad \rho_0 = 1.4 \quad q_0 = 0. \\ p_1 &= 1. \quad \rho_1 = 1. \quad q_1 = 0. \end{aligned}$$

Test 6:

$$\begin{aligned} p_0 &= 1. \quad \rho_0 = 1.4 \quad q_0 = .1 \\ p_1 &= 1. \quad \rho_1 = 1. \quad q_1 = .1 \end{aligned}$$

In all figures the solid curves are the exact solutions.

For Test 1 we compare LFC with HLLC in Figure 12a. Around the shock and the contact they behave in the same way, but the contact-corrected LF is less accurate than HLLC in the rarefaction wave. In Figure 12b we compare LW with LWC. LWC significantly reduces the oscillations of LW behind the contact, but has a larger overshoot at the shock.

For Test 2 LW and LWC fail. In Figure 13a we show the internal energy resulting from the scheme resulting from composing LFC and LWC, as described in [5]. Call this LWCn. We do n-1 time steps of LWC follwed by one step of LFC. In this case n=7 gave the best result. This is a difficult problem, as there is a near vacuum around the center. Most methods computed in [10] have a far greater error in the internal energy than does our composite. However, this is not entirely satisfactory since there is a large variation in behavior around n=7.

For Test 3 we show the density for LWC.

LWC runs Test 4, but has severe oscillations. Instead, we show the result of LWC3 together with HLLC. Note that Toro points out that LW fails on Test 3 and Test 4.

For Tests 5 and 6, LFC and LWC produce identical results and these are identical to those obtained from HLLC in Figure 10.9 of [10]. We show Test 5 only.

There are some other test problems that show that being exact for stationary contact discontinuities can be a mixed blessing. For the following data there is a shock with the fluid at rest behind the shock.

Simple shock:

$$\begin{aligned} p_0 &= .029 \quad \rho_0 = .138 \quad q_0 = 1.206 \\ p_1 &= .3 \quad \rho_1 = .5323 \quad q_1 = 0. \end{aligned}$$

Figure 15a shows a significant error near the position of the initial discontinuity at time $t = .5$. It seems here that there is no mechanism to dissipate the error left near the stationary trivial contact discontinuity, although

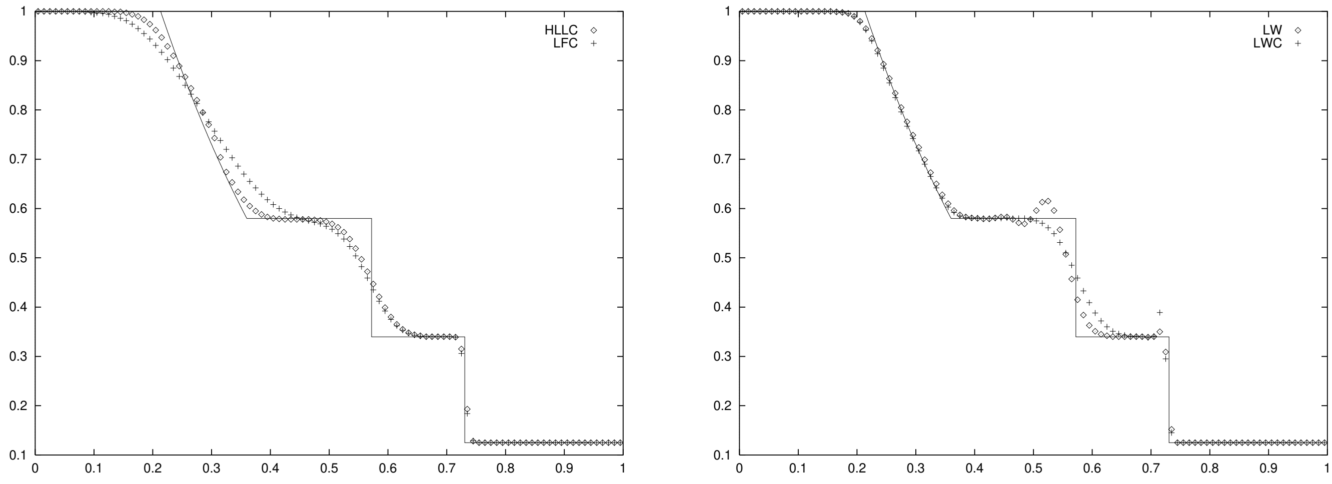

a) b)

Figure 12: Test 1, density, time = .2. a) LFC and HLLC; b) LW and LWC.

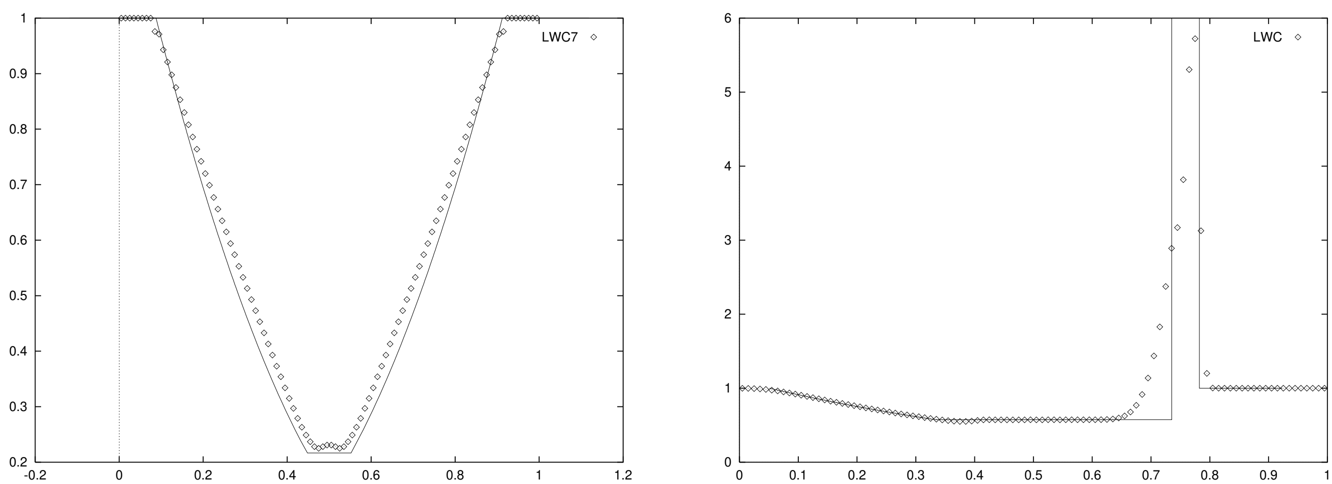

a) b)

Figure 13: a) Internal energy, Test 2, LWC7, time = .15. b) Density: Test 3, LWC, time = .012

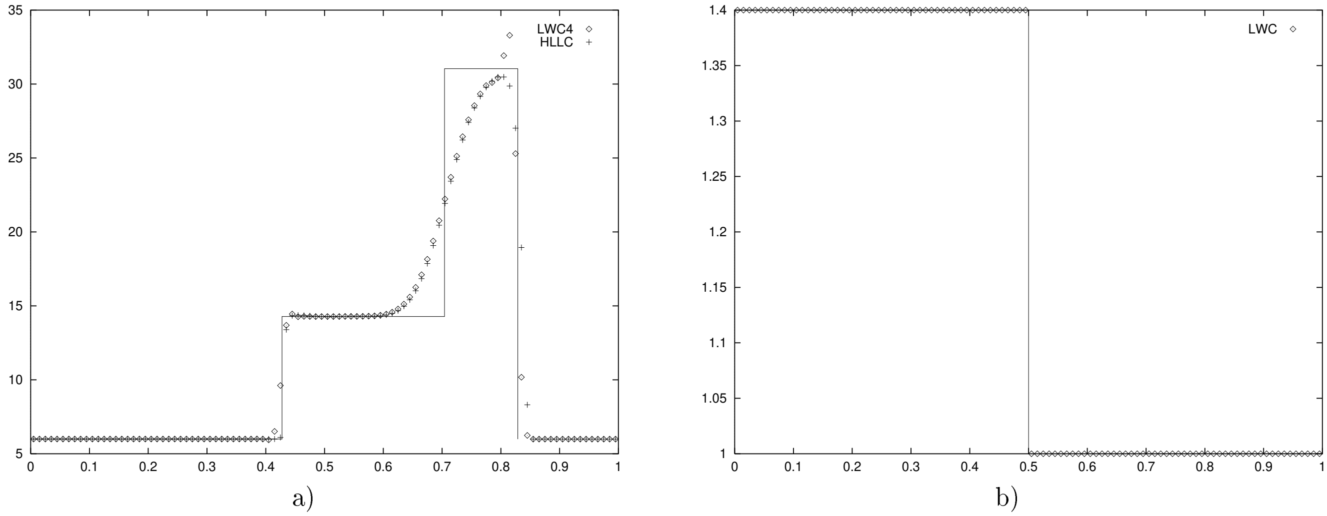

Figure 14: Density: Test 4, LWC4 and HLLC, time = .035: b) Density, Test 5, LWC, time = .2

HLLC works better on this problem than LWC. This phenomenon seems to be well known (E.F. Toro, private communication). See, for example, [11], [7], and[6].

Part of the difficulty here is that these difference schemes are not Galilean invariant. For all of these Riemann problems adding a constant to the initial velocities does not change the exact final thermodynamic states, but it definitely affects the numerical results. Toro has suggested the following Riemann problem which has a stationary contact.

Toro's high flow velocity problem:

$$\begin{aligned} p_0 &= 30. \times 10^6 \quad \rho_0 = 2. \quad q_0 = -3019.5071 \\ p_1 &= 10^5 \qquad \rho_1 = 1. \quad q_1 = -3019.5071 \end{aligned}$$

This is apparently difficult for some methods, but LWC4 does quite well with it, see Figure 15b.

6 Contact Correction in 2D

This is the third part of this work. The previous section shows that there may be sufficient improvement when contact discontinuities are modeled in HLL-type schemes that it might be worthwhile to try to do this in two dimensions.

6.1 Dimensionally split scheme using LFC and LWC

As an easy preliminary to a full development, and to have a basis for comparison, we present the result of using a dimensionally split 2D version of the contact-corrected composite LWCn. The composition is of $\mathrm{LWC_xLWC_y}$ applied $n-1$ times followed by $\mathrm{LFC_xLFC_y}$.

We present a computation of Configuration 15a which is a modification of Configuration 15 of [8]). The data are

$$\begin{aligned} p_{00} &= .3 \quad \rho_{00} = .8 \qquad q^x_{00} = .0 \qquad q^y_{00} = 0. \\ p_{01} &= .4 \quad \rho_{01} = .5197 \quad q^x_{01} = -.7259 \quad q^y_{01} = 0. \\ p_{11} &= 1. \quad \rho_{11} = 1. \qquad q^x_{11} = .0 \qquad q^y_{11} = 0. \\ p_{10} &= .4 \quad \rho_{10} = .5313 \quad q^x_{10} = 0. \qquad q^y_{10} = .7276. \end{aligned}$$

This is arranged so that there are stationary contact discontinuities, with slip, at the bottom and left edges, a shock at the right edge, and a rarefaction wave at the top. Figure 16 compares the split composite with CFLF4. The composite exactly resolves the initial contact discontinuities, but there is noise (about a 6% error) left in the stationary flow behind the shock at the right, just as there was in Figure 15a.

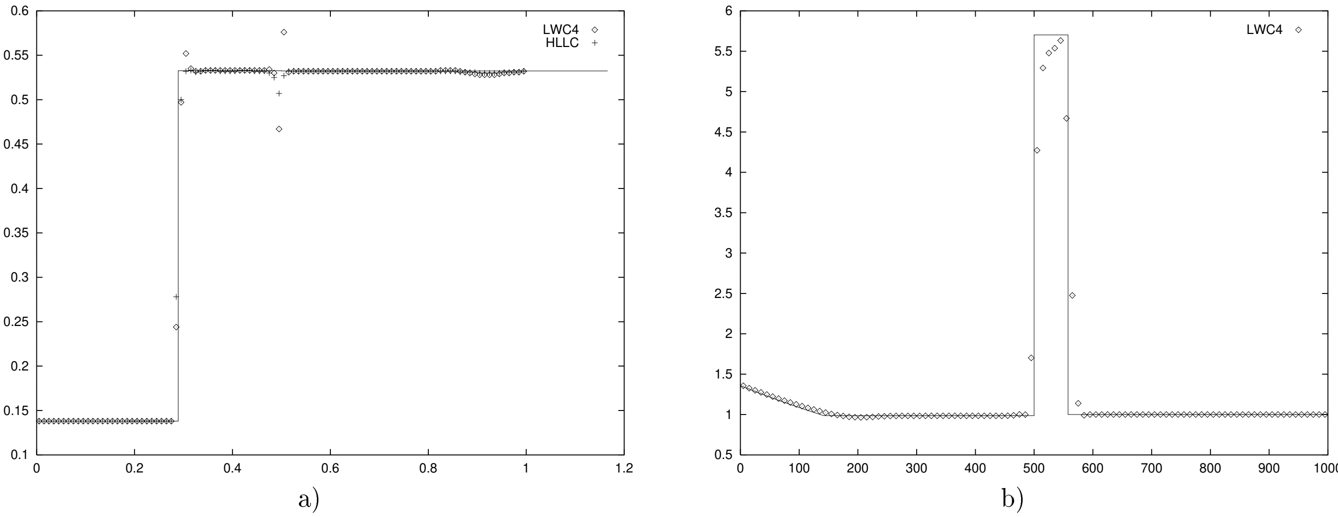

Figure 15: Density: a) Simple shock showing error for LWC4 and HLLC. b) High flow velocity stationary contact problem

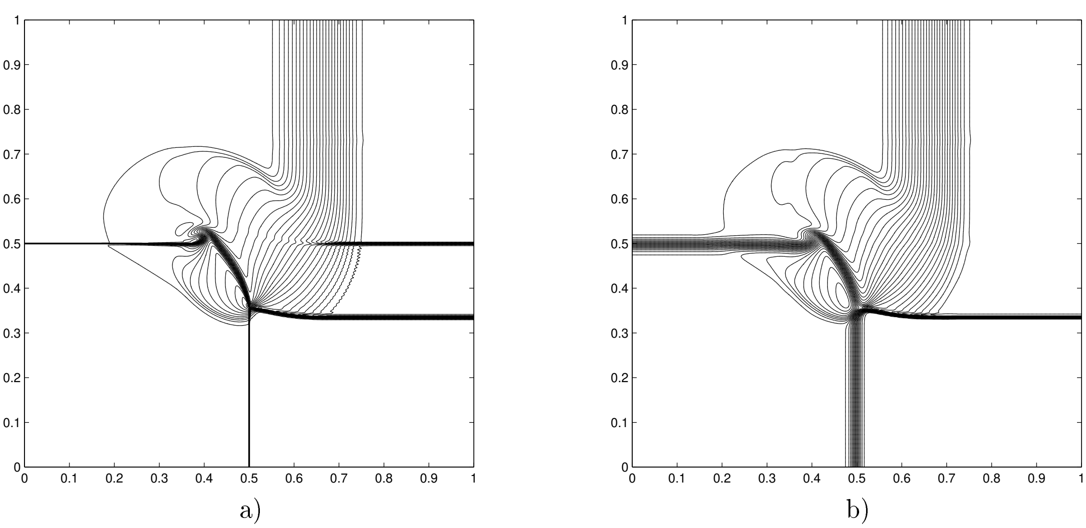

Figure 16: Configuration 15a. 400 × 400 grid, time=.2, cfl=.9, 30 density contours: a) Split composite. b) CFLF4
.

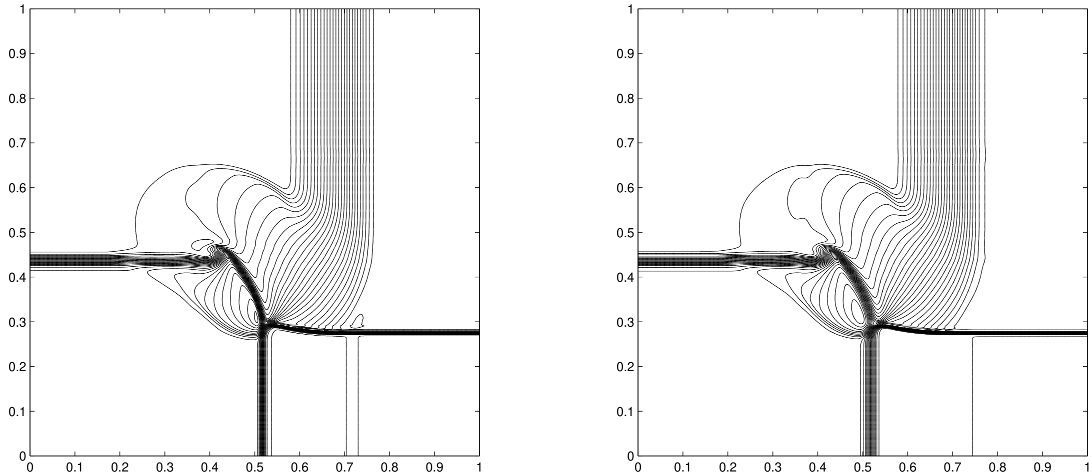

a) b)

Figure 17: Configuration 15. 400 × 400 grid, time=.2, cfl=.9, 30 density contours: a) Split composite. b) CFLF4
.

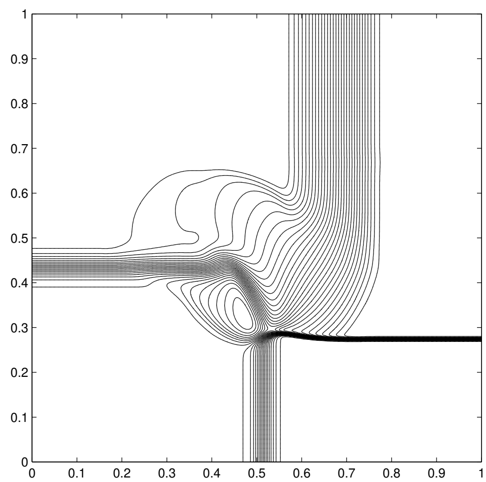

Figure 18: Configuration 15. 400 × 400 grid, time=.2, cfl=.9, 30 density contours: 2DHLLE

For the original Configuration 15 of [8]) the data are

$$\begin{array}{lllll} p_{00} & = & .3 & \rho_{00} = .8 & q^x_{00} = .1 & q^y_{00} = -.3 \\ p_{01} & = & .4 & \rho_{01} = .5197 & q^x_{01} = -.6259 & q^y_{01} = -.3 \\ p_{11} & = & 1. & \rho_{11} = 1. & q^x_{11} = .1 & q^y_{11} = -.3 \\ p_{10} & = & .4 & \rho_{10} = .5313 & q^x_{10} = 1 & q^y_{10} = .4276. \end{array}$$

This differs from 15a only in that the contact discontinuites are not stationary. The result is shown in Figure 17a for the split composite, and in Figure 17b for CFLF4. The composite shows slightly better resolution than CFLF4. The understandably poor performance of 2DHLLE on this problem is shown in Figure 18.

6.2 2D contact-corrected Lax-Friedrichs

Just as in 1D, a 2D version of Lax-Friedrichs can be obtained as a special case of HLLE using maximal speeds and two half steps. The LF scheme in [5] is the result; it has one state instead of nine. In spite of the fact that there are difficulties with the notion of contact correction we have attempted to create a 2D version of LFC. If that were successful it would be fairly easy to extend it to a 2D HLLC, since whatever procedure is used in the dual cell for LFC could be used in the central state of HLLE, while the 1D edge states would just be split in two by the 1D contact discontinuities. We have been able to construct a four-state 2D LFC, but one that is not entirely satisfactory. For this reason, and also because it would involve 16 states and be rather inefficient, we have not at this time followed up with a 2D HLLC.

The 2D LFC will be a two-step process, as in 1D. We give a brief partial description of the first half-step.

We require of a 2D LFC two properties: It should reduce to 1D LFC if the data is 1D, and it should be as simple as possible. The latter requirement means that we should not have to compute intersections of arbitrary quadrilaterals. We have arrived at the following procedure to accomplish this. The idea is to create two internal (to the dual cell) space time surfaces that will be treated as moving grid surfaces, but not necessarily as contact surfaces. These will divide the dual cell into four rectangular sub-cells, in analogy with the two intervals in LFC. The surfaces are defined by a velocity (U, V), to be chosen. Let the dual cell center be at (0,0). One surface is obtained by translating the line $x = 0$ horizontally with speed U, the other by translating the line $y = 0$ vertically with speed V. The lines $x = U\Delta t/2$, $y = V\Delta t/2$ together with the boundaries of the dual cell form the four regions of the dual cell at the half step. Each region will have a different density, but there will be one horizontal velocity in each horizontal strip, one vertical velocity in each vertical strip. Then each quadrant will have a density, and two momenta. Total mass and momenta in the dual cell are conserved. The pressure is obtained from the total energy and the kinetic energy in each quadrant.

First, let us define U and V. Refer to Figure3. Let U_N,respectively U_S, be the mean LF horizontal velocity connecting the states with indices (01) and (11), respectively (00) and (10). N and S refer to the north (upper) and south (lower) portions of the dual cell, at time $n + \frac{1}{2}$. Similarly, also at $n + \frac{1}{2}$, let V_E, respectively V_W, be the mean LF vertical velocity connecting the states with indices (10) and (11), respectively (00) and (01). E and W refer to the east (right) and west (left) portions of the dual cell. Then set

$$U \equiv \frac{1}{2}(U_N + U_S) \qquad\qquad V \equiv \frac{1}{2}(V_E + V_W).$$

Another possibility is to take U and V to be the 2D LF velocity components. In either case, if the data is independent of y then $U_N = U_S = U$, $V_E = q^y_{11} = q^y_{10}$, and $V_W = q^y_{01} = q^y_{00}$. An analogous statement holds if the data is independent of x.

We apply the integral conservation law for density in each quadrant, taking into account the moving internal surface. For example, for the northeast quadrant, after dividing by $\frac{1}{4}\Delta x\Delta y$, we have an equation of the form

$$(1 - \lambda U)(1 - \mu V)\rho_{NE} = \rho_{11} + \lambda((U_N - U)\rho_N - F^1_{NE}) + \mu((V_E - V)\rho_E - G^1_{NE}), \tag{36}$$

where F^1_{NE} and G^1_{NE} are the (normalized) integrated exterior partial boundary mass fluxes, and ρ_N and ρ_E are approximate integrated densities at the internal surfaces. ($\lambda = \Delta x/\Delta t, \mu = \Delta y/\Delta t$.) In order to maintain conservation the exact form of the fluxes depends on the relative sizes of U, U_N, U_S, and of V, V_E, and V_W. Suppose for example that $U \geq U_N$, $U \geq U_S$, and $V \geq V_E$. Then

$$G^1_{NE} = (\rho q^y)_{11}\frac{1 - \frac{1}{2}\lambda q^x_{11}}{1 - \frac{1}{2}\lambda U_N}(1 - \frac{1}{2}\lambda U),$$

$$\rho_E = \frac{1}{2}[\rho_{11}\frac{1 - \frac{1}{2}\lambda q^x_{11}}{1 - \frac{1}{2}\lambda U_N}(1 - \frac{1}{2}\lambda U) + \rho_{10}\frac{1 - \frac{1}{2}\lambda q^x_{10}}{1 - \frac{1}{2}\lambda U_S}(1 - \frac{1}{2}\lambda U)],$$

and

$$F^1_{NE} = (\rho q^x)_{11}\frac{1 - \frac{1}{2}\mu q^y_{11}}{1 - \frac{1}{2}\mu V_E}(1 - \frac{1}{2}\mu V).$$

Suppose the data are independent of y. Then $V_E\rho_E = G^1_{NE}$ and

$$\begin{aligned}(1 - \lambda U)(1 - \mu V)\rho_{NE} &= \rho_{11} - \lambda F^1_{NE} - \mu V\rho_E \\ &= \rho_{11}[1 - \lambda(1 - \frac{1}{2}\mu V)q^x_{11} - \mu V(1 - \frac{1}{2}\lambda q^x_{11}) \\ &= \rho_{11}(1 - \lambda q^x_{11})(1 - \mu V)\end{aligned}$$

which is the desired result.

The equation for the horizontal momentum in the north strip has the form

$$\begin{aligned}(1-\mu V)(\bar{\rho}\bar{q}^x)_N &= \frac{1}{2}(\rho q^x)_{01} + (\rho q^x)_{11}) + \frac{1}{2}\lambda(F^2_{NW} - F^2_{NE}) \\ &+ \mu(\frac{1}{2}[(V_E - V)(\rho U)_E + (V_W - V)(\rho U)_W)] - G^2_N) \end{aligned} \tag{37}$$

where F^2 and G^2 are the integrated x-component momentum fluxes. Again assuming $U \geq U_N$, $U \geq U_S$, $V \geq V_E$, and $V \geq V_W$ we have

$$\begin{aligned} F^2_{NE} &= [(\rho(q^x)^2)_{11}\frac{1-\frac{1}{2}\mu q^y_{11}}{1-\frac{1}{2}\mu V_E} + p^*_E](1-\frac{1}{2}\mu V), \\ F^2_{NW} &= [(\rho(q^x)^2)_{01}\frac{1-\frac{1}{2}\mu q^y_{01}}{1-\frac{1}{2}\mu V_W} + p^*_W](1-\frac{1}{2}\mu V), \\ G^2_N &= U_N(\rho q^y)_N, \end{aligned}$$

where p^*_E, p^*_W are average pressures for the east and west pairs of states, $(\rho q^y)_N$ is the LF average y-momentum for the north pair of states at $n+\frac{1}{2}$ and

$$\begin{aligned} (\rho U)_E &= \frac{1}{2}[U_N\rho_{11}\frac{1-\frac{1}{2}\lambda q^x_{11}}{1-\frac{1}{2}\lambda U_N}(1-\frac{1}{2}\lambda U) + U_S\rho_{10}\frac{1-\frac{1}{2}\lambda q^x_{10}}{1-\frac{1}{2}\lambda U_S}(1-\frac{1}{2}\lambda U)], \\ (\rho U)_W &= \frac{1}{2}[U_N(\rho_{01}(1+\frac{1}{2}\lambda q^x_{01}) + \frac{1}{2}\lambda(U-U_N)\rho_{11}\frac{1-\frac{1}{2}\lambda q^x_{11}}{1-\frac{1}{2}\lambda U_N}) + U_S(\rho_{00}(1+\frac{1}{2}\lambda q^x_{00}) + \frac{1}{2}\lambda(U-U_S)\rho_{10}\frac{1-\frac{1}{2}\lambda q^x_{10}}{1-\frac{1}{2}\lambda U_N})]. \end{aligned}$$

The horizontal velocity in the north strip is then

$$\bar{q}^x_N = \frac{(\bar{\rho}\bar{q}^x)_N}{\frac{1}{2}[(1-\lambda U)\rho_{NE} + (1+\lambda U)\rho_{NW}]}.$$

The complete description of all the quantities in all cases is too lengthy to include here.

For the second half step the masses and momenta are projected onto the primary cells. A single pressure, p^*, in the dual cell is obtained by subtracting the kinetic energy $\mathcal{K}$ from the total energy of the cell, where, in analogy with 1D LFC,

$$\begin{aligned} \mathcal{K} &= .125[(1-\mu V)(1-\lambda U)\rho_{NE}((\bar{q}^x_N)^2 + (\bar{q}^y_E)^2) + (1+\mu V)(1-\lambda U)\rho_{SE}((\bar{q}^x_S)^2 + (\bar{q}^y_E)^2) \\ &+ (1-\mu V)(1+\lambda U)\rho_{NW}((\bar{q}^x_N)^2 + (\bar{q}^y_W)^2) + (1+\mu V)(1+\lambda U)\rho_{SW}((\bar{q}^x_S)^2 + (\bar{q}^y_W)^2)] \end{aligned}$$

The fluxes at the center of the dual cell are obtained from the quantities in whichever quadrant that point lies. Finally, the projection of the energy is $p^*/(\gamma-1)$ plus half [the projection of ρq^x]^2 plus half [the projection of ρq^y]^2 all divided by the projection of ρ.

We show the result of computing with this 2D LFC on the two examples, configurations 15a and 15, compared with 2D Lax-Friedrichs, in Figures 19 and 20. There are clearly false signals propagating from the center out along the 1D contact discontinuities. We did a test, not shown, with 1D data and a small perturbation at the center, and similar signals were seen.

7 Remarks

We have presented a truly two-dimensional version of Godunov's method using an approximate 2D Riemann solver inspired by [4]. In its present form it is not really competitive with other methods for 2D compressible flow, but we hope it will stimulate research in this area. We have also offered 1D and 2D versions of the Lax-Friedrichs scheme designed to improve the resolution of contact discontinuites, with mixed results, but also with the hope of suggesting further research.

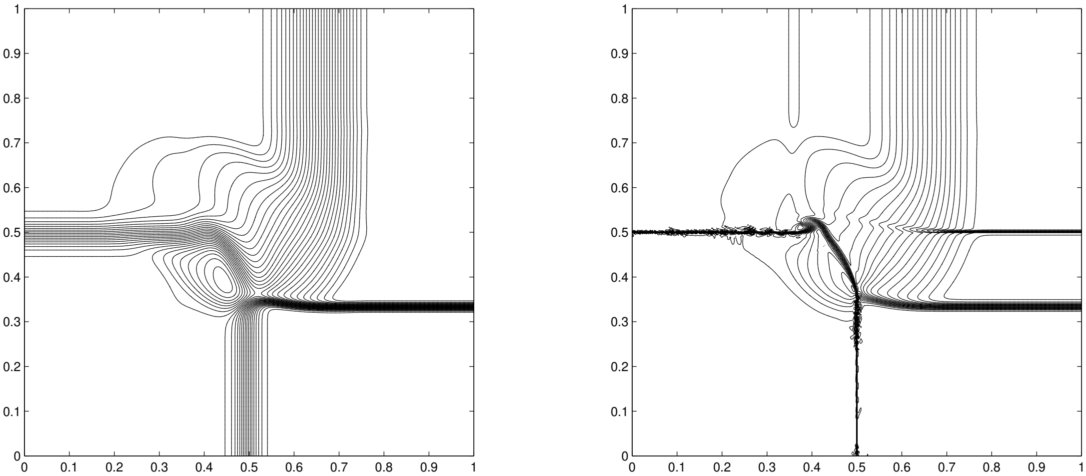

a) b)

Figure 19: Configuration 15a. 400 × 400 grid, time=.2, cfl=.9, 30 density contours: a) LF. b) 2DLFC

.

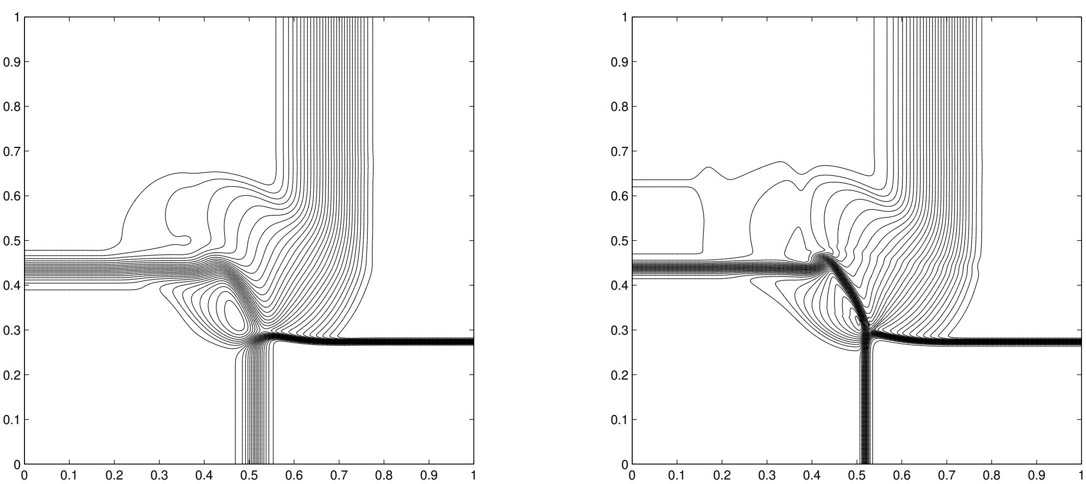

a) b)

Figure 20: Configuration 15. 400 × 400 grid, time=.2, cfl=.9, 30 density contours: a) LF. b) 2DLFC

.

8 Appendix A: 2D Einfeldt Speeds

The 1D Roe averages and speeds for the 2D equations can be found in [10] along with original references. We present them here for completeness.

Let

$$\begin{aligned} H_{i,j} &= \frac{1}{\rho_{i,j}}(E_{i,j} + p_{i,j}), \\ c_{i,j} &= \sqrt{(\gamma - 1)(H_{i,j} - .5((q^x_{i,j})^2 + (q^y_{i,j})^2))}. \end{aligned}$$

Then

$$\begin{aligned} \bar{q}^x_{i+\frac{1}{2},j} &= \frac{\sqrt{\rho_{i,j}}q^x_{i,j} + \sqrt{\rho_{i+1,j}}q^x_{i+1,j}}{\sqrt{\rho_{i,j}} + \sqrt{\rho_{i+1,j}}}, \\ \bar{q}^y_{i+\frac{1}{2},j} &= \frac{\sqrt{\rho_{i,j}}q^y_{i,j} + \sqrt{\rho_{i+1,j}}q^y_{i+1,j}}{\sqrt{\rho_{i,j}} + \sqrt{\rho_{i+1,j}}}, \\ \bar{H}_{i+\frac{1}{2},j} &= \frac{\sqrt{\rho_{i,j}}H_{i,j} + \sqrt{\rho_{i+1,j}}H_{i+1,j}}{\sqrt{\rho_{i,j}} + \sqrt{\rho_{i+1,j}}}, \\ \bar{c}_{i+\frac{1}{2},j} &= \sqrt{(\gamma - 1)(\bar{H}_{i+\frac{1}{2},j} - .5(((\bar{q}^x_{i+\frac{1}{2},j})^2 + (\bar{q}^y_{i+\frac{1}{2},j})^2))}. \end{aligned}$$

Then define the speeds:

$$\begin{aligned} b^1_{i+\frac{1}{2},j} &= \max(\bar{q}^x_{i+\frac{1}{2},j} + \bar{c}_{i+\frac{1}{2},j}, q^x_{i+1,j} + c_{i+1,j}) \\ b^0_{i+\frac{1}{2},j} &= \min(\bar{q}^x_{i+\frac{1}{2},j} - \bar{c}_{i+\frac{1}{2},j}, q^x_{i,j} - c_{i,j}). \end{aligned}$$

The speeds $b^1_{i,j+\frac{1}{2}}$, $b^0_{i,j+\frac{1}{2}}$ are obtained by interchanging the indices in all the doubly indexed quantities above, then interchanging i and j and then interchanging q^x and q^y.

9 Appendix B: Flux Form

We present here the flux form for method 3,

$$v^{n+1}_{i,j} = v^n_{i,j} - \frac{\Delta t}{\Delta x}(\mathcal{F}_{i+\frac{1}{2},j} - \mathcal{F}_{i-\frac{1}{2},j}) - \frac{\Delta t}{\Delta y}(\mathcal{G}_{i,j+\frac{1}{2}} - \mathcal{G}_{i,j-\frac{1}{2}})$$

without proof. This is a little easier to do in terms of lengths and areas rather than speeds. So, let

$$L^\bullet_{i+\frac{1}{2},j} = |b^\bullet_{i+\frac{1}{2},j}|\Delta t, \qquad L^\bullet_{i,j+\frac{1}{2}} = |b^\bullet_{i,j+\frac{1}{2}}|\Delta t, \qquad L^\bullet_{i+\frac{1}{2},j+\frac{1}{2}} = |d^\bullet_{i+\frac{1}{2},j+\frac{1}{2}}|\Delta t,$$

and

$$\begin{aligned} A^{00}_{i+\frac{1}{2},j+\frac{1}{2}} &= L^{x-}_{i+\frac{1}{2},j+\frac{1}{2}} L^{y-}_{i+\frac{1}{2},j+\frac{1}{2}}, \qquad A^{01}_{i+\frac{1}{2},j+\frac{1}{2}} = L^{x-}_{i+\frac{1}{2},j+\frac{1}{2}} L^{y+}_{i+\frac{1}{2},j+\frac{1}{2}}, \\ A^{11}_{i+\frac{1}{2},j+\frac{1}{2}} &= L^{x+}_{i+\frac{1}{2},j+\frac{1}{2}} L^{y+}_{i+\frac{1}{2},j+\frac{1}{2}}, \qquad A^{10}_{i+\frac{1}{2},j+\frac{1}{2}} = L^{x+}_{i+\frac{1}{2},j+\frac{1}{2}} L^{y-}_{i+\frac{1}{2},j+\frac{1}{2}}. \end{aligned}$$

The area of the central rectangle of the dual cell at $(i + \frac{1}{2}, j + \frac{1}{2})$ is

$$A_{i+\frac{1}{2},j+\frac{1}{2}} = A^{00}_{i+\frac{1}{2},j+\frac{1}{2}} + A^{01}_{i+\frac{1}{2},j+\frac{1}{2}} + A^{11}_{i+\frac{1}{2},j+\frac{1}{2}} + A^{10}_{i+\frac{1}{2},j+\frac{1}{2}}$$

Also

$$A^{00}_{i+\frac{1}{2},j+\frac{1}{2}} A^{11}_{i+\frac{1}{2},j+\frac{1}{2}} = A^{01}_{i+\frac{1}{2},j+\frac{1}{2}} A^{10}_{i+\frac{1}{2},j+\frac{1}{2}} \tag{38}$$

Let us first define cell fluxes to put into

$$v^{n+1}_{i,j} = v^n_{i,j} - \frac{\Delta t}{\Delta x}(\mathcal{F}^r_{i,j} - \mathcal{F}^l_{i,j}) - \frac{\Delta t}{\Delta y}(\mathcal{G}^r_{i,j} - \mathcal{G}^l_{i,j}).$$

Then we will just verify that

$$\mathcal{F}^r_{i,j} = \mathcal{F}^l_{i+1,j}, \quad \mathcal{G}^r_{i,j} = \mathcal{G}^l_{i,j+1},$$

so that

$$\begin{aligned} \mathcal{F}_{i+\frac{1}{2},j} &= \mathcal{F}^r_{i,j}, \quad \mathcal{F}_{i-\frac{1}{2},j} = \mathcal{F}^l_{i,j}, \\ \mathcal{G}_{i,j+\frac{1}{2}} &= \mathcal{G}^r_{i,j}, \quad \mathcal{G}_{i,j-\frac{1}{2}} = \mathcal{G}^l_{i,j}. \end{aligned}$$

Consider $\Delta y \Delta t \mathcal{F}^r_{i,j}$, which can be split into three parts:

$$\Delta y \Delta t \mathcal{F}^r_{i,j} = Z^r_1 + Z^r_2 + Z^r_3, \tag{39}$$

and correspondingly,

$$\Delta y \Delta t \mathcal{F}^l_{i,j} = Z^l_1 + Z^l_2 + Z^l_3. \tag{40}$$

Z^r_1 is the flux at $(i+\frac{1}{2}, j)$ coming from the normal Riemann problem at this edge. There is a contribution to it from the dual cells at $(i+\frac{1}{2}, j+\frac{1}{2})$ and at $(i+\frac{1}{2}, j-\frac{1}{2})$. It is

$$Z^r_1 = \frac{\Delta y - L^{y-}_{i+\frac{1}{2},j+\frac{1}{2}} - L^{y+}_{i+\frac{1}{2},j-\frac{1}{2}}}{L^{x+}_{i+\frac{1}{2},j} + L^{x-}_{i+\frac{1}{2},j}} [L^{x+}_{i+\frac{1}{2},j} L^{x-}_{i+\frac{1}{2},j} (v_{i,j} - v_{i+1,j}) + \Delta t (L^{x+}_{i+\frac{1}{2},j} f_{i,j} + L^{x-}_{i+\frac{1}{2},j} f_{i+1,j})]. \tag{41}$$

Then Z^l_1 is just Z^r_1 with i replaced by $i-1$ and x^- interchanged with x^+. These clearly have the needed left right symmetry.

Z^r_2 comes from the same dual cells, but it contains the terms arising from the 2D intermediate dual states that are independent of f and g. It is

$$\begin{aligned} Z^r_2 &= \frac{A^{00}_{i+\frac{1}{2},j+\frac{1}{2}}}{A_{i+\frac{1}{2},j+\frac{1}{2}}} [\frac{1}{2} A^{11}_{i+\frac{1}{2},j+\frac{1}{2}} (v_{i,j+1} - v_{i+1,j+1} + v_{i,j} - v_{i+1,j}) + A^{10}_{i+\frac{1}{2},j+\frac{1}{2}} (v_{i,j} - v_{i+1,j})] \\ &+ \frac{A^{01}_{i+\frac{1}{2},j-\frac{1}{2}}}{A_{i+\frac{1}{2},j-\frac{1}{2}}} [\frac{1}{2} A^{10}_{i+\frac{1}{2},j-\frac{1}{2}} (v_{i,j-1} - v_{i+1,j-1} + v_{i,j} - v_{i+1,j}) + A^{11}_{i+\frac{1}{2},j+\frac{1}{2}} (v_{i,j} - v_{i+1,j})] \end{aligned} \tag{42}$$

For Z^l_2 replace i by $i-1$, and in the first superscript of the $A's$ interchange 0 and 1. Then (38) provides the left right symmetry.

Z^l_3 contains the remaining contributions from the two dual cells. First, let

$$\begin{aligned} \hat{F}^+_{0,\frac{1}{2}} &= \frac{1}{2}(2d^{y+}_{\frac{1}{2},\frac{1}{2}} - b^+_{0,\frac{1}{2}} \Delta t) \Delta t f(u_{01}) + \frac{1}{2} b^+_{0,\frac{1}{2}} (\Delta t)^2 f(u_{0,\frac{1}{2}}), \\ \hat{F}^-_{0,\frac{1}{2}} &= \frac{1}{2}(2|d^{y-}_{\frac{1}{2},\frac{1}{2}}| + b^-_{0,\frac{1}{2}} \Delta t) \Delta t f(u_{00}) + \frac{1}{2}(-b^-_{0,\frac{1}{2}}) (\Delta t)^2 f(u_{0,\frac{1}{2}}), \\ \hat{F}_{0,\frac{1}{2}} &= \hat{F}^+_{0,\frac{1}{2}} + \hat{F}^-_{0,\frac{1}{2}} \end{aligned}$$

and

$$\begin{aligned} \hat{G}^+_{\frac{1}{2},0} &= \frac{1}{2}(2d^{x+}_{\frac{1}{2},\frac{1}{2}} - b^+_{\frac{1}{2},0} \Delta t) \Delta t g(u_{10}) + \frac{1}{2} b^+_{\frac{1}{2},0} (\Delta t)^2 g(u_{\frac{1}{2},0}), \\ \hat{G}^-_{\frac{1}{2},0} &= \frac{1}{2}(2|d^{x-}_{\frac{1}{2},\frac{1}{2}}| + b^-_{\frac{1}{2},0} \Delta t) \Delta t g(u_{00}) + \frac{1}{2}(-b^-_{\frac{1}{2},0}) (\Delta t)^2 g(u_{\frac{1}{2},0}), \\ \hat{G}_{\frac{1}{2},0} &= \hat{G}^+_{\frac{1}{2},0} + \hat{G}^-_{\frac{1}{2},0}. \end{aligned}$$

Then in analogy with (9) it can be shown that

$$\begin{aligned} A_{\frac{1}{2},\frac{1}{2}} u_{\frac{1}{2},\frac{1}{2}} &= A^{00}_{\frac{1}{2},\frac{1}{2}} u_{00} + A^{01}_{\frac{1}{2},\frac{1}{2}} u_{01} + A^{10}_{\frac{1}{2},\frac{1}{2}} u_{10} + A^{11}_{\frac{1}{2},\frac{1}{2}} u_{11} \\ &+ [\hat{F}_{0,\frac{1}{2}} - \hat{F}_{1,\frac{1}{2}}] + [\hat{G}_{\frac{1}{2},0} - \hat{G}_{\frac{1}{2},1}]] \end{aligned} \tag{43}$$

Then Z_3^r has a part from the dual cell at $(i+\frac{1}{2}, j+\frac{1}{2})$, namely,

$$
\begin{aligned}
Z_{3a}^r &= \frac{|dy^-_{i+\frac{1}{2},j+\frac{1}{2}}|}{(|dy^-_{i+\frac{1}{2},j+\frac{1}{2}}| + dy^+_{i+\frac{1}{2},j+\frac{1}{2}})A_{i+\frac{1}{2},j+\frac{1}{2}}}[(A^{00}_{i+\frac{1}{2},j+\frac{1}{2}} + A^{01}_{i+\frac{1}{2},j+\frac{1}{2}})(\hat{F}_{i+1,j+\frac{1}{2}} - \hat{G}^+_{i+\frac{1}{2},j} + \hat{G}^+_{i+\frac{1}{2},j+1}) \\
&+ (A^{10}_{i+\frac{1}{2},j+\frac{1}{2}} + A^{11}_{i+\frac{1}{2},j+\frac{1}{2}})(\hat{F}_{i,j+\frac{1}{2}} - \hat{G}^-_{i+\frac{1}{2},j} + \hat{G}^-_{i+\frac{1}{2},j+1})]
\end{aligned} \tag{44}
$$

The part from the dual cell at $(i+\frac{1}{2}, j-\frac{1}{2})$, Z_{3b}^r, is obtained from Z_{3a}^r by interchanging dy^- with dy^+, and replacing j by $j-1$. Then $Z_3^r = Z_{3a}^r + Z_{3b}^r$. To get Z_3^l interchange 0 with 1 in the first superscript of the A's, interchange $\hat{G}^+$ with $\hat{G}^-$, and replace i by $i-1$. Again, the necessary left right symmetry is present.

To define the $\mathcal{G}$ fluxes, it is only necessary to make appropriate substitutions. First, in (39.40) replace $\mathcal{F}$ by $\mathcal{G}$. In (41,42,44) interchange y with x (e.g., dy becomes dx, L^x becomes L^y), interchange f with g and F with G. Then interchange subscripts, and i with j (.e.g. $v_{i,j+1}$ becomes $v_{i+1,j}$). Next, interchange superscripts in the $A's$. These interchanges must also be made when obtaining the Z^l quantities.

References

[1] P. Batten, N. Clarke, C. Lambert, and D. M. Clauson, On the choice of wavespeeds for the HLLC Riemann solver, *SIAM J. Sci. Comput.* **18** , 1553-1570 (1997).

[2] B. Einfeldt, On Godunov-type methods for gas dynamics, *SIAM J. Numer. Anal.* **25**, 294-318 (1988).

[3] B. Einfeldt, C. D. Munz, P. L. Roe, and B. Sjøgreen, On Godunov-type methods near low densities, *J. Comp. Phys.* **92**, 273-295 (1991).

[4] A. Harten, P. D. Lax and B. van Leer, On upstream differencing and Godunov-type schemes for hyperbolic conservation laws, *SIAM Rev.* **25**, 35-61 (1983).

[5] R. Liska and B. Wendroff, Composite schemes for conservation laws, *SIAM J. Numer. Anal.* **35**, 2250-2271 (1998).

[6] S. Obayashi and Y. Wada, Practical formulation of a positively conservative scheme, *AIAA J.* **32**, 1093-1095 (1994).

[7] T. W. Roberts, The behavior of flux difference splitting schemes near slowly moving shock waves, *J. Comp. Phys.* **90**, 2250-2271 (1990).

[8] C. W. Schulz-Rinne, J. P. Collins, and H. M. Glaz, Numerical solution of the Riemann problem for two-dimensional gas dynamics, *SIAM J. Sci. Comput.* **14**, 1394–1414 (1993).

[9] J. Smoller, Shock Waves and Reaction Diffusion Equations, Springer, 1994

[10] E. F. Toro, Riemann Solvers and Numerical Methods for Fluid Dynamics, Springer, 1997

[11] Y. Wada and M-S. Liou, An accurate and robust flux splitting scheme for shock and contact discontinuities, *SIAM J. Sci. Comput.* **18**, 633–657 (1997).

[12] B. Wendroff, A Two-dimensional HLLE Riemann Solver and Associated Godunov-Type Difference Scheme for Gas Dynamics, *Los Alamos National Laboratory Report* LAUR 98-5490, to appear in Computers and Mathematics with Applications.